INTERNATIONAL ATOMIC ENERGY AGENCY
UNITED NATIONS EDUCATIONAL, SCIENTIFIC AND CULTURAL ORGANIZATION
INTERNATIONAL CENTRE FOR THEORETICAL PHYSICS
I.C.T.P., P.O. BOX 586, 34100 TRIESTE, ITALY, CABLE: CENTRATOM TRIESTE

H4.SMR/942-31

Third Workshop on 3D Modelling of Seismic Waves Generation Propagation and their Inversion

4 - 15 November 1996

Waveform Inversion for Source Parameters

P. Suhadolc

Department of Earth Sciences
Trieste, Italy

Inversion of waveforms for extended-fault kinematic parameters

Introduction

Solution of an inverse problem is required to interpret any measurements that are indirect like inferences of the properties of the Earth's interior and of the seismic source. The basic measurements of seismology are, in fact, arrival times and amplitudes of different phases, or better, time series of ground motion. These data are controlled by both the elastic and inelastic properties of the Earth, as well as the properties of the source exciting the Earth. Inversion is a formal way to make inferences about these properties.

The zeroth-order requirement for solution of any inverse problem is that before one can hope to solve the inverse problem, one has to be able to solve the "forward problem". This means that one has to understand the physical processes that produced the observation well enough to make a reliable mathematical model of the process. The forward problem can be written schematically as

$$d_i = F_i\,[m(r)]$$

where $m(r)$ is a model describing some physical property of the Earth, d_i i sthe predicted value for datum i and F_i is a functional whose existence implies that if we know m exactly, we could predict the data perfectly.

This is the simplest class of inverse solutions, the forward modelling, involving an educated guess (or a trial and error procedure) to derive an m that fits all the observable data according to some defined measure of goodness of fit (e.g., a chi-square test, minimum fit according to some norm etc.). The fundamental weakness of this procedure is that once a model is found that fits the data, one does not know how reliable that model is.

The fundamental difference between the construction of an inverse procedure compared to forward modelling is that the data are used directly to construct a solution. We can write this formally as:

$$m(r) = F_i^{-1}\,[d_i\,]$$

Every inverse problem should address the following aspects:

Existence:	Does any model fit the data?
Uniqueness:	Can the data uniquely constrain the model?
Construction:	How can we find a solution?
Appraisal:	How well do the data constrain the model.

Usually little attention is paid to the first two and much of the efforts go to the third aspect, the construction. Sometimes even the fourth aspect is neglected, which should be the most significant feature of a good inverse procedure. It answers the question of how good the solution one constructs really is.

Most of the work done so far on this problem was concentrated on the third aspect and only in recent years several researchers have focussed on the fourth aspect. In fact, finding a solution means nothing. The focus of a good analysis must lie with apprasing the nonuniqueness of the solution.

Since even by obtaining the global-minimum solution one does not know, when working with real data, how close the obtained solution is to the "real" one, I will show for the case of extended faults, how one can investigate the quality and non-uniqueness of the solution by inverting artificially generated data.

Setup of the problem and general considerations

Problem:

Given the time series of motion recorded at a certain number of station around the causative fault, find the temporal and space distribution of slip on the fault.

Using standard inverse methods it is not difficult to obtain a solution which fits the data acceptably well.

Past studies until some time ago have concentrated on deriving a model that fits the data, without assessing solution stability or resolution.

Parametrization:

Size of the cell
The rupture surface is subdivided into a grid work of small cells or subfaults.
They should be small enough in order for the solution to outline well the rupturing process, but on the other end as the number of cells increases, the stability of the problem decreases. The point-source spacing is such that the subfault synthetics look like a continuous rupture over the bandwidth of the inversion and not as a bunch of separate point-source releases. This is obvoiusly related to the minimum wavelength one wants to resolve in the problem or equivalently to the maximum frequency involved. Cells should be small enough in order for the time required to the rupture to traverse a subfault be significantly less than the predominant period content of the data. However also the directivity effect is important and a good check is therefore to make forward models with smaller and smaller cells until the seismograms at the given stations are stable.
If the subfault synthetics are computed before the inversion process is initiated, the speed of inversion increases significantly.

The focal mechanism is usually kept constant for all the cells, but some authors have tried to resolve both the dip and slip components at each cell; others have tried to resolve for the rise time at each cell.

The ground motion for a unit amount of slip on each subfault is computed by a time-domain sum of point sources. Each subfault synthetic is lagged in time and scaled in amplitude according to the present model estimation.

We have also to remember that the Green functions normally used are far-field approximate solutions. Attention should be paid that all the used stations are at a sufficient distance from the nearest element of the fault that this approximation is still valid. A few wavelengths away from the nearest element of the fault is usually sufficient.

It is assumed many times that an earthquake starts at a point and grows outward with a continuous rupture, i.e. the rupture may not jump. This last condition may be relaxed at predetermined fault segments. Some people do not make this assumptions and leave the fault to rupture spontaneously (with some causality constraints).
Rupture velocities usuallly range from 2 km/s to 4 km/s.

Rise times: cannot resolve rise times smaller than minimum period contained in the data.

Synthetics for the subfault containing the hypocenter are aligned with the first significant arrival from the source region. Possible small time shifts to account for the unknown structural model (which does not take into account lateral inhomogeneities).

Objective (or cost) function - Goodness of the solution

This is the function to be minimized in order to obtain an acceptable fit between the data and the model.

$$\sum_{i=1}^{N} W_i \int [\, x_i(t) - u_i(t) \,]^2 \, dt = \text{minimum}$$

with $x_i(t)$ the synthetics, $u_i(t)$ the data and W_i some weight given to the data.
This is the L2 norm, but also the L1 and other norms can be used. Even the choice of the norm can be an ambiguous decision (see e.g. differences between L1 and L2 norm solutions keeping all other aspects of the problem the same in Hartzell et al., 1991: BSSA, 81, 1518-1539), but generally the choice is not a critical one.

Without weighting, close stations with larger seismogram amplitudes dominate the least-squares inversion (e.g. Frankel, 1992: BSSA, 82, 1511-1518).

Instability and non-uniqueness

Increasing the model dimension results in a decrease of the solution uniqueness.
To stabilize the problem external constraints need to be placed on the inverison.

The parametrization itself severly restricts the possible solutions and has a big stabilizing effect. Discretization of the fault with a limited number of cells, restricted to slip in a limited time interval.

Attention: a too restrictive parametrization can lead to the true solution lying outside the solution space of the model.

Need to parametrize the problem with sufficient flexibility to encompass realistic models of faulting: ---> physical constraints serve to stabilize the inversion.

Physical constraints are desirable stabilizing tools because they can be unambiguously stated and easily adapted to reflect the current knowledge of the earthquake source physics.

Some techniques require the use of several initial random models to verify that the solution is stable with respect to the starting model and inversion procedure.
Important to understand what factors affect the solution.

Resolution

Absolute resolution is difficult to address, because one can evaluate the resolution only for the specific problem, not for the actual earthquake source.
Therefore, usual resolution matrices (Menke, 1984) are of limited value and can give only relative estimates of error.

One way is to compare solutions that utilize different data sets, parametrizations, constraints, and inversion norms.
In terms of fitting the data many solutions give an equally acceptable model. The similarities of these different solutions are considered to be the aspects of the rupture model that are better resolved, in an absolute sense.

Robustness

Use different methods --> the common features of these solutions point out robust characteristicss of the slip distribution that are independent of the inversion parametrization.

Dissimilarities in the solutions for 1989 Loma Prieta discussed by Wald et al., 1991: BSSA, 81, 1540-1572 (stations used, data weighting, to less extent Green functions?)

For 1992 Landers by Hartzell and Liu, 1996: PEPI, 95, 79-99 --> actual inversions
For 1992 Landers by Cohee and Beroza, 1994: AdG, 37, 1515-1538 by using synthetic test.

Single-window vs. multi-window inversion

Single-window inversion --> Fukuyama and Irikura, 1986: BSSA, 76, 1623-1640
Takeo, 1987: BSSA, 77, 490-513
Beroza and Spudich, 1988: JGR, 93, 6275-6296
Hartzell and Iida, 1990: JGR, 95, 12475-12485

In the single-window method asumes that each point ruptures only once, when the rupture front passes. Rupture time variations are allowed by admitting perturbations to a constant-rupture-velocity model. The perturbations are found in a separate, nonlinear inversion. Rise time is assumed to be constant and optimized by finding the value which produces the best overall fit to the data.

Multi-time-window inversion --> Olson and Apsel, 1982: BSSA, 72, 1969-2001
Hartzell and Langer, 1993: JGR, 98, 22123-22134
Hartzell et al. 1994: BSSA, 84, 1703-1724

In these inversions each point on the fault is allowed to rupture multiple times.

The single-window method tends to recover the true seismic moment and the average rupture velocity.
Linear inversions with multiple-time-window tend to overestimate the moment with respect to single-time-window inversions.
Neither can resolve temporal details of the rupture propagation, unless constraints from independent data (e.g. from geodesy) are applied.
For a comparison between the two methods see e.g.:
Cohee and Beroza, 1994: AdG, 37, 1515-1538

If in term of the ability to fit the data some parametrization (e.g. variable rise time) is not required, than drop it.

Physical constraints

Positivity of slip
Strong causality (limits on rupture velocity)
Weak causality (rupture velocity smaller than P-wave velocity)
Model fits observed surface offsets
Tapering of slip to zero at the bottom of the fault
Find least moment or predetermined moment model
Model which incorporates minimum and maximum limits on rupture velocity

Other constraints

Find spatially smoothest model
Find minimum norm model

Incorporated as limits to the current model or as linear functions appended to the calculation of the objective function.

Brief review of the work done in this field

A review of different extended-fault inversions with respect to some proposed parametrizations is given below.

Each cell is allowed to rupture according to a preset timing. The assumption of a constant rupture velocity is implied, leading to a linear problem.

Trifunac, 1974: BSSA, 64, 149-172	1971 San Fernando
Hartzell et al., 1991: BSSA, 81, 1518-1539	1989 Loma Prieta

The slip in each subfault is discretized in time. This allows for a variable rise-time function on the fault.

Olson and Apsel, 1982: BSSA, 72, 1969-2001	1979 Imperial valley
Hartzell and Heaton, 1983: BSSA, 73, 1553-1583	1979 Imperial valley
Hartzell and Langer, 1993: JGR, 98, 22123-22134	1974 Peru
Wald and Heaton, 1994: BSSA, 84, 668-691	1992 Landers
Mendoza et al., 1994: BSSA, 84, 269-283	1985 Central Chile
Hartzell et al. 1994: BSSA, 84, 1703-1724	North American eqs.

Use approximate Green functions, allowing for more time intervals

Frankel and Wenneberg, 1989: BSSA, 79, 515-541	1987 Superstition Hills

Solve for the timing, location and moment of a discrete sum of point sources, rather than employing a continuous rupture
This is a flexible method, since it deals wiht a discontinuous sequencing of sources
One has though no guarantee to find a global minimum and physical constraints are difficult to implement

Kikuchi and Kanamori, 1982: BSSA, 72, 491-506
Kikuchi and Kanamori, 1986: PEPI, 43, 205-222
Kikuchi and Kanamori, 1991: BSSA, 81, 2335-2350

The time domain formulation implies a nonlinear and multimodal problem, i.e. the objective function has more than one local minimum.
The problem is solved by linearizing it and using the iterative least squares.
Disatvantage: likely to find a local rather than global minimum.
Advantage: if the timing of the starting model is selected as the best-fitting constant rupture velocity from linar analysis, then the optimal solution in the neighbourhood of this model can be found.

Jackson and Matsu'ura, 1985: JGR, 90, 581-591	
Yoshida, 1986: JPE, 34, 235-255	
Fukuyama and Irikura, 1986: BSSA, 76, 1623-1640	1983 Akita-Oki
Takeo, 1987: BSSA, 77, 490-513	
Beroza and Spudich, 1988: JGR, 93, 6275-6296	1984 Morgan Hill
Hartzell, 1989: JGR, 94, 7515-7534	1986 North Palm Springs
Hartzell and Iida, 1990: JGR, 95, 12475-12485	1987 Whittier Narrows
Cohee and Beroza, 1994: AdG, 37, 1515-1538	1992 Landers

Solve the problem in the frequency domain

The calculation of rupture time and slip amplitude is linear and inversion for each freqency component is done separately. Physical constraints are however difficult to apply

Linearized, iterative, frequency-domain method

Cotton and Campillo, 1995: JGR, 100, 3961-3975 1992 Landers

Linear programming with L1 norm minimization

Used with only weak causality constraints on rupture times. Can incorporate many physical constraints and thus stablize the problem.

Das and Kostrov, 1990: JGR, 95, 6899-6913	1986 Andreanoff Isl.
Das and Kostrov, 1994: PEPI, 85, 293-318	1989 Macquarie Ridge
Das and Suhadolc, 1996: JGR, 101, 5725-5738	-
Das et al., 1996: TP, in press	-

Apply global search algorithms to the non-linear multimodal problem
Able to find global minimum, can apply time-domain cosntraints

Hybrid global search algorithm

Simulated annealing algorithm initially searches widely to find an appropriate model that is not far from the global minimum, then the downhill simplex method moves to the global minimum itself.

Liu et al., 1995: JGR 122, 991-1000
Hartzell and Liu, 1995: BSSA 85, 516-524
Hartzell and Liu, 1996: PEPI, 95, 79-99. 1992 Landers

Simulated annealing (SA)

Uses an analogy with physical annealing in thermodynamic systems: for slowly cooling sysems, nature is able to find minimum energy states.
Throughout the process the non-zero probability of long jumps allows the method to escape from local minima.
The method first searches widely (random walk) in model space (analog: high-temperature system), then the search is restricted and the algorithm freezes to the global minimum.

Metropolis et al., 1953: J. Chem. Phys., 21, 1087-1092.
Kirkpatrick et al., 1983: Science, 220, 671-680

Genetic algorithms (GA)

Unlike SA, an initial population of models is selected at random and the GA seks to improve the fit of the population generation after generation. This is accomplished by the genetic process of selection, crossover and mutation.

Holland, 1975: Adaptation in natural and artificial systems. U. of Michigan Press.

Goldberg, 1989: Genetic Algorithms in Search, Optimization and Machine learning, Addison Wesley.

Forrest, 1993: Genetic Algorithms: Principles of natural selection applied to computation.

Stoffa and Sen, 1991: Nonlinear multiparameter optimization using genetic algorithms: Inversion of plane wave seismograms. Geophysics, 56, 1794-1810.

Other strong motion data inversions

Mendez and Luco, 1990: JGR, 95, 327-340	California eqs.
Mendez and Anderson, 1991: BSSA, 81, 844-861	1985 Michoacan
Cocco and Pacor, 1993:TP, 218, 157-177	1980 Irpinia
Cotton and Campillo, 1994: AdG, 37, 1539-1564	1985 Michoacan, 1992 Landers

Other works on earthquake rupture on extended faults

Heaton, 1990: PEPI, 64, 1-20.	"Heaton pulse"
Langer and Hartzell, 1996: PEPI, 94, 121-132	1977 Western Argentina eq.
Hartzell and Heaton, 1986: BSSA, 76, 649-674	1984 Morgan Hill
Wald et al., 1990: BSSA, 80, 1079-1098	1987 Superstition Hills
Beroza, 1991: BSSA, 81, 1603-1621	1989 Loma Prieta
Steidl etal., 1991: BSSA, 81, 1573-1602	1989 Loma Prieta
Wald et al., 1991: BSSA, 81, 1540-1572	1989 Loma Prieta

JOURNAL OF GEOPHYSICAL RESEARCH, VOL. 101, NO. B3, PAGES 5725–5738, MARCH 10, 1996

On the inverse problem for earthquake rupture: The Haskell-type source model

S. Das

Department of Earth Sciences, University of Oxford, Oxford, England

P. Suhadolc

Istituto di Geodesia e Geofisica, Universita di Trieste, Trieste, Italy

Abstract. In order to gain insight into how to invert seismograms correctly to estimate the details of the earthquake rupturing process, we perform numerical experiments using artificial data, generated for an idealized faulting model with a very simple rupture and moment release history, and solve the inverse problem using standard widely used inversion methods. We construct synthetic accelerograms in the vicinity of an earthquake for a discrete analog of the Haskell-type rupture model with a prescribed rupture velocity in a layered medium. A constant level of moment is released as the rupture front passes by. We show that using physically based constraints, such as not permitting back slip on the fault, allow us to reproduce many aspects of the solution correctly, whereas the minimum norm solution or the solution with the smallest first differences of moment rates in space and time do not reproduce many aspects for the cases studied here. With the positivity of moment rate constraint, as long as the rupturing area is allowed to be larger than that in the forward problem, it is correctly found for the simple faulting model considered in this paper, provided that the rupture velocity and the Earth structure are known. If, however, the rupture front is constrained either to propagate more slowly or the rupturing area is taken smaller than that in the forward problem, we find that we are unable even to fit the accelerograms well. Use of incorrect crustal structure in the source region also leads to poor fitting of the data. In this case, the proper rupture front is not obtained, but instead a "ghost front" is found behind the correct rupture front and demonstrates how the incorrect crustal structure is transformed into an artifact in the solution. The positions of the centroids of the moment release in time and space are generally correctly obtained.

Introduction

With the deployment of high dynamic range, broad band digitally recording seismometers, and the availability of supercomputers, it has become feasible to consider the problem of inverting seismograms to obtain the details of the moment release time history and distribution on earthquake faults. The solution of this problem is important for the following reasons. Since the moment release on faults is generally expected to be nonuniform, one can identify regions of high and low moment release, or slip deficit. The slip or moment distribution obtained from such inversions can be used to infer the stress drop distribution due to the earthquake [e.g., *Miyatake*, 1992] that in turn can be used to estimate stress accumulation on faults. The slip deficit as well as the stress accumulation history on the fault can then lead to inferences about the times of future earthquakes on the fault. An example where a portion of a fault with slip deficit in one earthquake ruptured relatively soon afterwards in another earthquake is the 1986 Andreanof Islands earthquake [*Das*, 1990]. The rupture zone of the Andreanof Islands earthquake was contained entirely within that of the 1957 Aleutian earthquake ($M_w = 8.6$), yet the 1986 earthquake of $M_w = 8.0$ occurred only 29 years later on a plate boundary that is believed to have a much larger characteristic repeat time. Noting that the region of major moment release in the 1986 earthquake coincided with the region of the 1957 event that had essentially no aftershocks, *Das* [1990] identified the 1986 earthquake to be due to the slip deficit left after the 1957 event. Another situation in which the inverse problem solution is useful is when one can relate the variations in moment release on the fault to the morphology, say jogs or bends, or cross-cutting physical features on faults, and so on. Such understanding can lead in the long term to successful prediction of the expected ground motion at particular sites of special interest, say, the locations of critical structures such as power plants, dams, bridges, etc., in regions where large earthquakes are expected. Finally, once the motion on the fault is reconstructed, the entire displacement field can be found by solving the appropriate

Paper number 95JB03533.
0148-0227/96/95JB-03533$05.00

forward problem. This makes it possible to estimate the motion at some site where there is damage but where there was no seismometer [e.g., *Suhadolc et al.*, 1990], thus enabling the cause of the damage, for example, focusing of waves on the site, to be investigated.

The inverse problem for the earthquake source was first formulated by *Kostrov* [1970], and discussed by *Kostrov* [1975] and by *Kostrov and Das* [1988]. Of the numerous studies that estimate the rupture and moment release history during earthquakes, we mention here the papers that develop a new method, or extend an existing method of inversion for both the spatial and temporal moment release pattern on the fault. These include *Olson and Apsel* [1982], *Kikuchi and Kanamori* [1982], *Hartzell and Heaton* [1983], *Kikuchi and Fukao* [1985], *Beroza and Spudich* [1988], *Mendoza and Hartzell* [1988a, 1988b, 1989], *Olson and Anderson* [1988], *Das and Kostrov*, [1990, 1994], *Hartzell et al.* [1991], and *Hartzell and Liu* [1995].

The limitations of such inversions have, however, not yet been studied sufficiently. For example, how close is the solution of this problem, which is well known to be unstable, to the actual moment distribution? How does poor knowledge of crustal structure in the source region affect the estimate of the rupture front location and speed? Since such inversions are not unique, what methods can one use to choose the "correct" solution from among the multiplicity of solutions? The last question cannot, in fact, be answered when working with real data, since the actual moment release at the depths where earthquakes occur is unknowable. In their studies of the great 1986 Andreanof Islands earthquake and the great 1989 Macquarie Ridge earthquake, *Das and Kostrov* [1990, 1994] attempted, using teleseismic data, to choose solutions from among the many possible ones. They demonstrated that more than one slip distribution can fit the data equally well. For the Macquarie Ridge earthquake, alternative slip distributions that could be interpreted as due to a propagating crack or to isolated asperities rupturing fit the data. The different rupture models would clearly lead to different stress accumulation patterns and histories on the fault [*Ruff*, 1983].

In geophysical inverse problems, the solution is often stabilized by using nonphysical prior bounds, such as finding the minimum norm solution or the smoothest solution. *Hartzell and Heaton* [1983] and *Das and Kostrov* [1990,1994] investigated physically based constraints that can be used to stabilize the solutions. We shall show that physical constraints, such as not allowing back slip on the fault, produce the proper results, whereas the minimum norm solution and the solution with the smallest first differences do not, for the cases studied in this paper. *Hartzell and Heaton* [1983], *Mendoza and Hartzell* [1988a, 1988b, 1989], *Hartzell et al.* [1991], and *Hartzell and Liu* [1995] have used various stabilizing bounds in their inverse problem solutions and *Hartzell and Liu* [1995] summarize many features of such prior bounds.

In this paper we shall address only some specific aspects of the questions raised above by using artificial data where we do know what the correct solution is. We shall use the vertical components of synthetic accelerograms constructed using the "far-field" approximation in the vicinity of the earthquake epicenter for source receiver distances in the 15 to 35 km range, generated by a very idealized model of earthquake rupture. We shall take the fault rupture model to be a Haskell-type dislocation [*Haskell*, 1964, 1966, 1969] propagating at a constant rupture velocity. This model has the great advantage of being very simple and has been widely used in seismic source studies, both for the forward problem and for the inverse problem. *Madariaga* [1978] proved that it is an appropriate model for simulating radiation with wavelengths longer than the fault width, as in this paper. Some of the studies of the inverse problem referred to above use essentially this model. We therefore use this simple model to obtain insight into the inverse problem. In this study we confine ourselves to using accurate data and seismograms close to the earthquake source. We do not discuss the teleseismic problem, although some of the results could be adapted to that case by scaling of the fault size and wave periods used here. Neither do we discuss the effects of noise in the data. Rather, we aim to gain insight into the basic problem of solving such unstable inverse problems by studying a very simple and idealized situation. Most importantly, working with synthetic data provides the possibility of identifying artifacts of the solution and their causes.

We first set out briefly the method used to generate the synthetic ground motion data. We next describe the inverse solution method, generate many sets of synthetic data for different faulting models, invert them, and present the results. Finally, we examine the limitations of the inverse problem for earthquake faulting, identifying, for example, which source properties we might be able to infer reliably, which ones depend strongly on knowledge of proper crustal structure, and so on.

Description of the Mathematical Problem

The formulation of the problem in terms of the slip rate or slip on the fault is well known and is stated only briefly here. Using the representation theorem (e.g., equation (3.2) of *Aki and Richards* [1980]; equation (3.2.18) of *Kostrov and Das* [1988]) and neglecting body forces, the displacement record at a station located at point $\mathbf{x}_1$ on the Earth's surface can be expressed in terms of the slip distribution over a fault surface, Σ, as an integral equation of the first kind [*Das and Kostrov*, 1990]

$$u_k(\mathbf{x}_1, t_1) = \int_0^{t_1} dt \iint_\Sigma K_{ik}(\mathbf{x}_1, \mathbf{y}_1, t_1, t) a_i(\mathbf{y}_1, t) dS, \quad (1)$$

where $i, k = 1, 2, 3$, $u_k(\mathbf{x}_1, t_1)$ are the components of the displacement vector, $a_i(\mathbf{y}_1, t)$ are the components of the slip, and $K_{ik}(\mathbf{x}_1, \mathbf{y}_1, t_1, t)$ are the components of the impulse response of the medium at $(\mathbf{x}_1, t_1)$, due to a dislocation point source at $(\mathbf{y}_1, t)$. By moving the time derivative that exists in the kernel K to the slip term in (1), we obtain an equivalent representation in terms of the slip-rate distribution over the fault, with the corresponding kernel G. In short,

$$\mathbf{u} = K * \mathbf{a} = G * \dot{\mathbf{a}}, \quad \text{where} \quad K = \dot{G} \tag{2}$$

where $\mathbf{u}$ is the displacement vector, $\mathbf{a}$ and $\dot{\mathbf{a}}$ are the slip and slip rate vectors, respectively, asterisk denotes convolution over the fault area and source duration, and dot denotes time derivative. We shall assume that the fault is planar and that the slip direction is constant over the fault. We can use either form of (2) to find slip or slip rate, if we know the kernels K and G and the displacement seismograms. Slip rate is easily converted into moment rate given the modulus of rigidity.

Discretizing the problem, by dividing the fault into square cells and the source time function into steps, reduces (2) to the system of equations

$$A\mathbf{x} \approx \mathbf{b}, \tag{3}$$

where A is the matrix obtained by integrating G or K over fault cells and time steps, each column of A being the appropriate discretized set of the kernel for all stations corresponding to different cells and time instants, ordered in the same way as the observations $\mathbf{b}$, and $\mathbf{x}$ are the unknown slips or slip rates. In this paper, we use the formulation in terms of the slip rates and the kernel G.

The Green functions are determined using the multimodal summation method for a layered, anelastic medium [*Panza*, 1985; *Panza and Suhadolc*, 1987; *Florsch et al.*, 1991]. In this paper we shall only use the vertical component of motion and Rayleigh wave modal summation to determine the Green function kernel. We have chosen to work initially with the vertical component only to make the matrix A smaller, for a given number of stations. The effect of including the horizontal component on the inversion will be investigated in the future.

The medium consists of homogeneous layers separated by first-order discontinuities. The modal summation method allows exact and complete solution of the full wave equation for a laterally homogeneous medium in a preassigned (ω,c) interval, where ω is the angular frequency, and c is the phase velocity [e.g. *Aki and Richards*, 1980]. The seismic source is included in the computations using the formulation due to *Harkrider* [1964] and *Ben-Menahem and Harkrider* [1964]. The extended fault is modeled as a grid of point sources, and the synthetic seismogram at each station due to the moment release on the fault is computed by summing the contributions from each point source with appropriate delays and weights [*Panza and Suhadolc*, 1987].

In this paper the Green functions are computed for a maximum frequency of 1 Hz. The frequency domain is sampled with 200 points in the range DC to 1 Hz, which gives a frequency step of 0.005 Hz, yielding good frequency resolution between 0.1 Hz and 1 Hz. The upper frequency of 1 Hz implies minimum wavelengths on the order of 1 km for the velocity models considered in this paper. The achievable spatial resolution on the fault at a given instant of time is on the order of 0.5 km. The size of the time step used in constructing the Green functions is taken as about 0.1 s (more precisely as 200/2048=0.09765 s, where 200 is the number of points in the frequency domain and 2048 is the number of points in the discrete Fourier transform).

Construction of the Synthetic Data

The synthetic accelerograms to be used in the inversion are constructed by performing the convolution in (2) for the particular faulting models considered. In this study the forward problem is a discretized form of the Haskell dislocation propagating unilaterally over a rectangular fault at a constant rupture velocity, $v_r = 0.7v_S$, where v_S is the shear wave speed in the medium. Figure 1 shows the fault geometry together with a schematic diagram of the propagating rupture. The fault is taken to be of pure dip-slip type with a 30° dip and with the top of the fault located at a depth of 1 km below the Earth's surface.

The discrete approximation (3), of equation (1), must be fine enough to be a good approximation to the integral in (1), must be representative for the wave lengths involved in the data, and yet be feasible to solve. The spatial cell size Δx

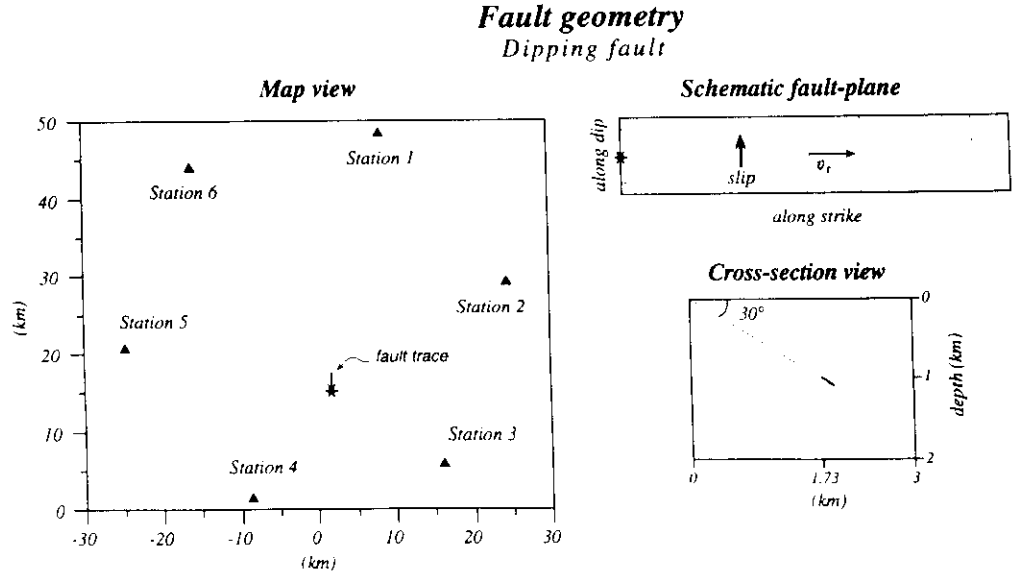

Figure 1. Fault and station geometry.

Table 1. Summary of Inversion Method, Parameters, and Results

Case	Source Medium (inv)	Faulting Parameters: Top of Fault (inv, km)	nh (fwd)	nh (inv)	nt (fwd)	nt (inv)	Centroid[a] in time (fwd)	Constraints Used	Inversion Method	Centroid[a] in Time (inv)	Centroid[b] Along Strike (inv)	Remarks
1a	$M1$	1	1	1	21	21	10.5	$R1(0.7v_S)$,MTO	SVD	10.6	26.0	Only total moment correctly reproduced
(2)	$M1$	1	1	1	21	21	10.5	$R1(0.7v_S)$,MTO,P	LP	10.5	25.5	Entire solution correctly reproduced
1b	$M1$	1	1	1	21	21	10.5	$R2$,MTO	SVD	10.6	26.0	Same as case 1a
(2)	$M1$	1	1	1	21	21	10.5	$R2$,MTO,P	LP	10.5	25.5	Entire solution reproduced
1c	$M1$	1	1	1	21	21	10.5	$R1(0.5v_S)$,MTO,P	LP	9.8	17.3	Poor solution
1d	$M1$	1	1	1	21	21	10.5	$R1(0.5v_S)$,MTO,P,M	LP	9.9	17.3	" "
2a	$M1$	1	1	5	21	21	10.5	$R1(0.7v_S)$,P	LP	10.6	26.0	Some aspects of solution correct
(2)	$M1$	1	1	5	21	21	10.5	$R1(0.7v_S)$,P,MTO	LP	10.4	25.5	Entire solution correctly reproduced
2b	$M1$	1	5	1	21	21	10.5	$R1(0.7v_S)$	LP	10.9	26.2	Some aspects of solution correct
(2)	$M1$	1	5	1	21	21	10.5	$R2$	LP	10.3	23.9	Rupture front correctly found
3a	$M2$	2.05	1	1	21	38	10.5	$R2$,MTO,P	LP	20.3	24.3	Poor solution
3b	$M2$	2.05	1	5	21	38	10.5	$R2$,MTO,P	LP	11.1	20.3	" "

$nx = 51$; $\Delta x = 50m$; $\Delta t = 0.097..s$ in all forward (fwd) and inverse (inv) cases.
FORWARD PROBLEM: Centroid along strike, measured from hypocenter/Δx=25.5; source in medium $M1$.
[a]Time centroid is $/\Delta t$. [b]Centroid along strike is $/\Delta x$.
MTO is "more than once".
For meaning of other constraints, see text.

on the fault is taken as 50 m and the time step size Δt in the source time function as approximately 0.1 s, both for the forward and inverse problems. The rupture front is discretized using the same spatial and temporal gridding, with the moment being released at the center of each cell and in the middle of each time step as the rupture front crosses any portion on the cell within the time step interval. The moment is released only once in each cell, at the time the cell ruptures. The level of moment released at each cell is taken as constant and equal to 1 x 10^{11} N m. The problem using finer discretization in the forward than in the inverse problem is the subject of another paper [*Das et al.*, 1995].

The size of the fault varies in the different cases considered here. Table 1 summarizes the length and width of the rupture area for each case. Figure 2 shows velocity profiles with depth for the Earth structures $M1$ and $M2$ that we shall use in this study. $M1$ has a low velocity layer that is absent in $M2$. The Q values in the two models range from a value of 20 in the surficial layers to 100 in the deep sediments and 400 beneath them. The six stations, distributed equally in azimuth around the fault (Figure 1), are chosen so as not to involve nodal directions. The hypocenter is marked by a star and the source receiver distances lie in the 15 to 35 km range. All the synthetic accelerograms are sampled at the same time interval as the time step size used to construct the Green function, about 0.1 s, and the entire accelerogram is used in the inversion.

Solution of the Inverse Problem

Since the integral equation (1) is unstable, we need to stabilize it by the use of additional constraints. *Olson and Apsel* [1982], *Hartzell and Heaton* [1983], *Das and Kostrov* [1990, 1994], and *Hartzell and Liu* [1995], among others, have identified constraints that can be used for this purpose. The physically based constraints we shall use in this paper are as follows:

1. Slip rate $\mathbf{x} \geq 0$ for all points on the fault for all time ("positivity" constraint P).
2. The final moment must equal some preassigned value ("moment" constraint M).
3. The rupture is constrained to move at, or more slowly than, some preassigned speed ("strong causality" constraint $R1$). It is important to point out that there is no rupture criterion involved in the discrete inverse problem, and by "rupture speed" we mean the rupture speed of some (unspecified) rupture triggering signal.
4. The moment rate is zero in any cell and time step that would produce a signal before the first arrival at any station from the hypocentral cell ("weak causality" constraint $R2$). In the case when there is insufficient station coverage, if this constraint is used without the constraint $R1$ also being enforced, the inversion may permit super P "rupture speeds".
5. In the forward problem, moment is released only once as the cell breaks. In the inverse problem, a cell may be allowed to release moment more than once. The phrase 'more than once' (MTO) will be used to denote this case.

We select constraints for the different cases studied (Table 1) in order to to gain insight into the effects on the solution of the constraints. Constraints of this type have been called "hard prior bounds" by *Jackson* [1979] and *Backus* [1988].

In addition, it is possible to improve the stability of the problem by the use of "soft prior bounds", such as finding the solution with the minimum norm or the smoothest solution in some sense, say, the solution with the smallest first differences. This is done by adding a term to the penalty functional $||\mathbf{b} - A\mathbf{x}||_p$, where $p = 1, 2, ...$, as desired. For example, to obtain the minimum norm solution, one then minimizes $||\mathbf{b} - A\mathbf{x}||_p + \eta||\mathbf{x}||_p$, where η is some weighting factor. To find the solution with the smallest first difference (in space and/or time), one minimizes $||\mathbf{b} - A\mathbf{x}||_p + \eta$ times the chosen norm of the appropriate first differences of $\mathbf{x}$, and so on. Such stabilizations have been used in the papers on inverse problem solution referred to earlier.

To solve the constrained linear system (3), we shall use two standard methods, discussed by *Press et al.* [1986], *Tarantola* [1987], and *Parker* [1994]. First, we solve (3) using the method of singular value decomposition (SVD), in which we minimize $||\mathbf{b} - A\mathbf{x}||_2$. If the results are not satisfactory, for example, if the moment obtained in not the right one, then we again use SVD but constrain the moment to a preassigned value (constraint M). If the results are still not satisfactory, for example, if there are large negative moment rates on the fault, we remove small singular values and examine the solution. Finally, in some instances we shall find the solution with the smallest first differences in space and time and compare it with the correct solution. In the second approach, we solve (3) using various combinations of the physical constraints discussed above and the method of linear programming, in which the 1-norm of the penalty functional

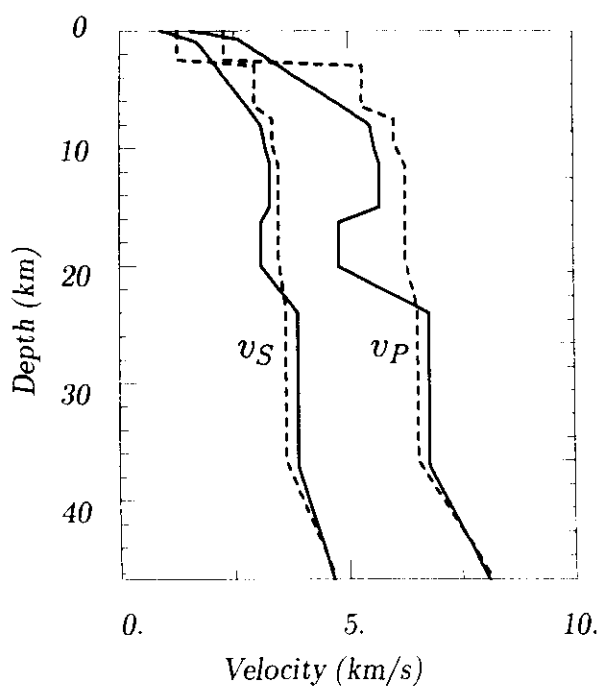

Figure 2. The P and S wave velocity profiles with depth in the crust for medium $M1$ (solid line) and medium $M2$ (dashed line).

is minimized. In some instances when using this second approach, we shall find solutions with the smallest second differences, following the formulation developed and applied to the earthquake faulting problem by *Das and Kostrov* [1990, 1994]. For some cases we use only the second approach to solve the inverse problem. The inversion method used together with the constraints and the results obtained for each case are summarized in Table 1.

Results

More than 40 inversions were performed. Selected cases are discussed in detail below.

Case 1

The synthesized vertical accelerograms in this case correspond to a unilateral rupture that spreads out over a 2.55 km-long and 50 m-wide fault in 21 time steps with a rupture velocity of $v_r = 0.7v_S$ in $M1$. The number of cells (nx) along fault strike is 51 and the number (nh) along the fault dip is 1. The number of time steps will be denoted by nt. The shortest wavelength (about 1.2 km for this case) is much larger than the fault width. Figure 3 shows the rupture model, the moment rate history and distribution and the final moment over the fault for this forward problem. (The corresponding source time function is shown later in Figure 5a.) The six synthesized accelerograms are displayed in Figure 4. Simply in order to check our programs, we solve this problem with the same rupture model and the the same Earth structure as in the forward problem. The system of equations has 51 unknowns and about 1500 equations (sum of all the samples in all the accelerograms) and is an exact one. A simple unconstrained SVD solution is found to agree with the forward problem to machine accuracy.

Case 1a: Rupture front constrained to actual front. We next constrain the rupture velocity v_r to be the same as in the forward problem ($0.7v_S$), but without restricting the number of times each cell behind the rupture front releases moment (MTO). The number of unknowns is now 554. The unconstrained SVD solution is close to the moment rate distribution of Figure 3 but with some negative values behind the rupture front, the magnitude of these moment rates being about 1% of the constant moment rate level of the forward problem. The solution fits the accelerograms to several significant figures. The solution source time function is compared to the true one in Figure 5a. For the first few time steps, when the area of slip on the fault is not large, the agreement is good, but at later times the source time function obtained oscillates about the correct solution. Though the total moment is correctly reproduced without being constrained, the final moment distribution on the fault, plotted in Figure 5b, also oscillates around the actual solution. Thus the negative moment rates, though small, when summed in space to produce the source time function or in time to obtain the final moment, have a nonnegligible contribution. Excluding small singular values did not improve the situation significantly. The centroids of the moment distribution in time and along strike are shown in Table 1. Both centroids are found to be close to the correct ones.

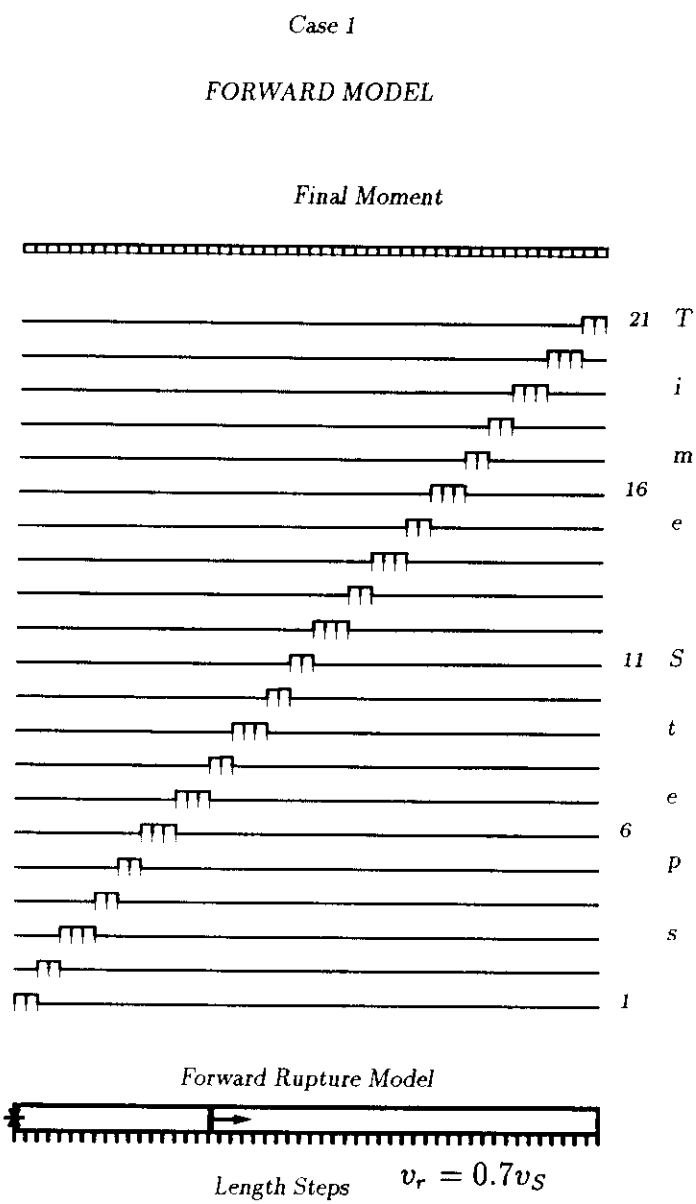

Figure 3. The forward model for case 1. The rupture model is displayed at the bottom of the figure, the moment rate time history along the fault length above it and the final moment along the fault is illustrated at the top. The fault length is taken along the abscissa and time is plotted along the ordinate. The numbers at the right indicate the time step. The level of moment release at each cell is 1 x 10^{11} N m. The cells that are slipping at each time step are indicated by tick marks below the trace. The scales used for plots similar to this will be kept the same throughout the paper to facilitate comparison, though the shift between time steps might vary in later figures in the interest of clarity. The solutions of the inverse problems for case 1, case 2a, and case 3 should be compared to this figure.

We next find the solution with the smallest first differences in space and time, but are still unable to remove the large number of small negative moment rates from the solution. We then solve the problem using linear programming and

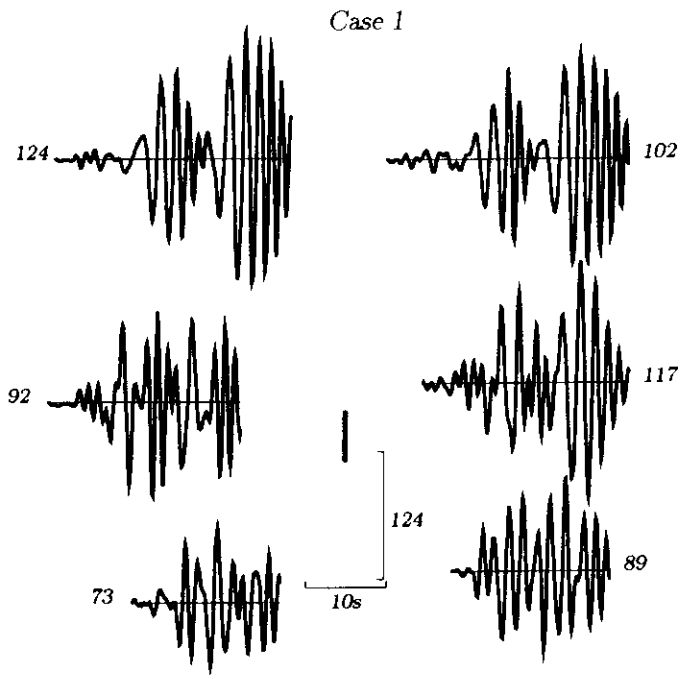

Figure 4. The synthetic accelerograms for the fault and station geometry of Figure 1, for the forward model of case 1. The thick line is the fault strike and the numbers next to each accelerogram give the maximum ground acceleration, multiplied by 100, in centimeters per second squared.

enforcing the moment rate to be positive (Case 1a(2)). All aspects of the forward model are now reproduced exactly. Even though cells have the freedom to release moment during more than one time step, it is found that each cell releases moment only once. Thus for the simple rupture model used here, we can reproduce the moment rate distribution and history on the fault if we know the rupture front, the focal mechanism and fault geometry, and Earth structure, by constraining the moment rate to be positive but without constraining the total moment. Since the predicted accelerograms cannot be distinguished from the original accelerograms (Figure 4), they are not plotted.

Case 1b: Weak causality applied to rupture front. We next apply the weak causality constraint (*R2*), with cells behind the causal front being allowed to release moment as often as necessary (MTO). We solve the inverse problem using both SVD and linear programming. The number of unknowns is now 987. The conclusions are the same as in case 1a. Thus as long as the positivity constraint is enforced, we can reproduce the rupture process using the weak causality constraint, knowing the fault mechanism, the fault geometry, and the Earth structure.

Case 1c: Rupture front constrained to propagate more slowly than in the forward problem. We next consider the same problem as in case 1a, but constrain the rupture front to a velocity of $0.5v_S$. We use only the linear programming approach in this case. The moment is not constrained and cells are allowed to release moment as often as necessary, but the moment rate is constrained to be positive. The number of unknowns is now 398. Owing to the low rupture speed con-

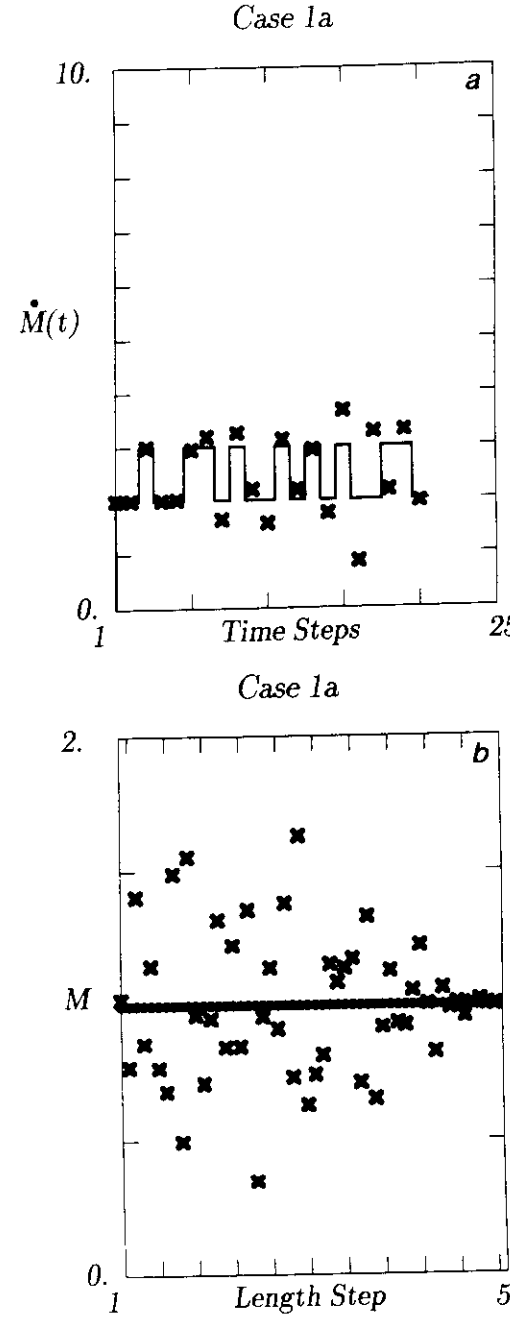

Figure 5. (a) Moment release per time step, multiplied by 1 x 10^{11} N m, on the fault for the forward problem (solid line) and the solution (crosses) for case 1a. In the forward problem either two or three cells break at each time step. The number of cells allowed to break at each time step is the same in the forward and in the inverse problem in this case, but the figure demonstrates that the amount of moment released at each time step in the inversion does not agree with that in the forward problem. (b) Final moment distribution, multiplied by x 10^{11} N m, on the fault for the forward problem (dots) and the solution (crosses) for case 1a.

straint used in the inversion, only part of the fault can rupture in the total rupturing time, which is determined by the durations of the synthetic accelerograms. Figure 6 shows the forward and inverse rupture models and the moment rate history obtained. Figure 7a shows the fit to the data; the fit is not per-

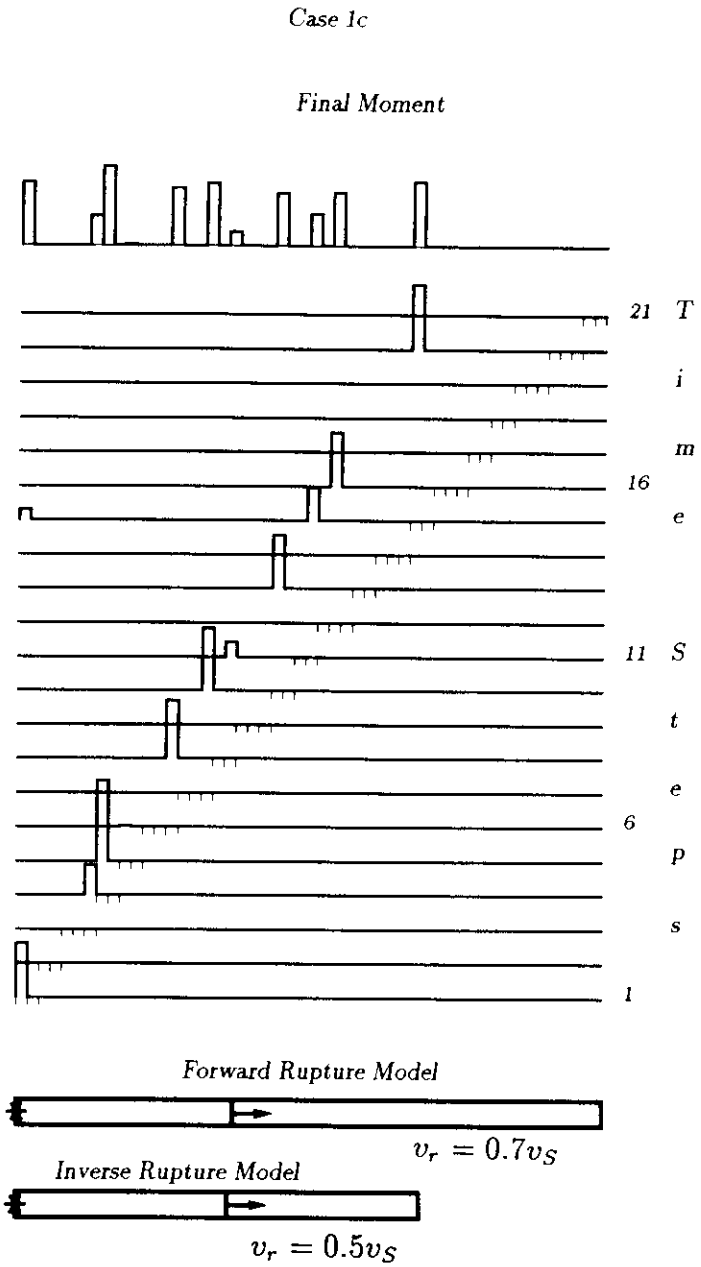

Figure 6. Same as Figure 3 but for the inversion in case 1c. Compare with Figure 3.

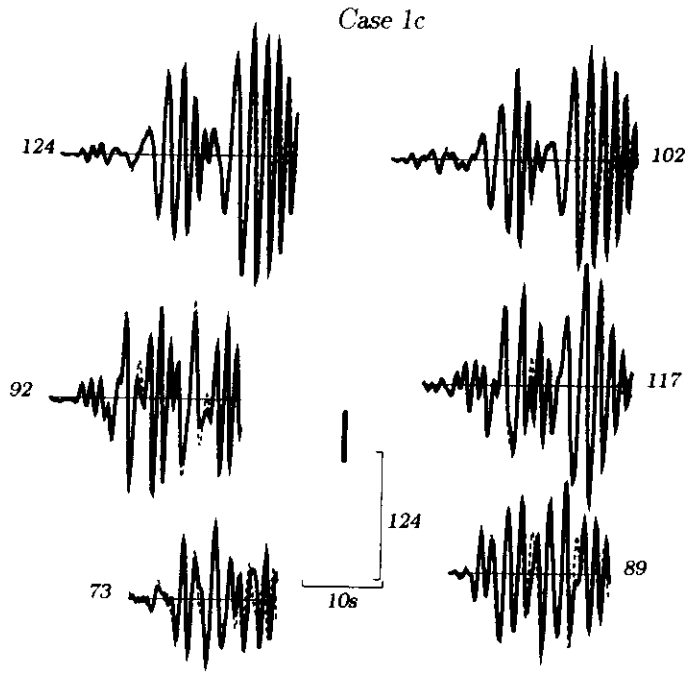

Figure 7a. Same as Figure 4 but for case 1c.

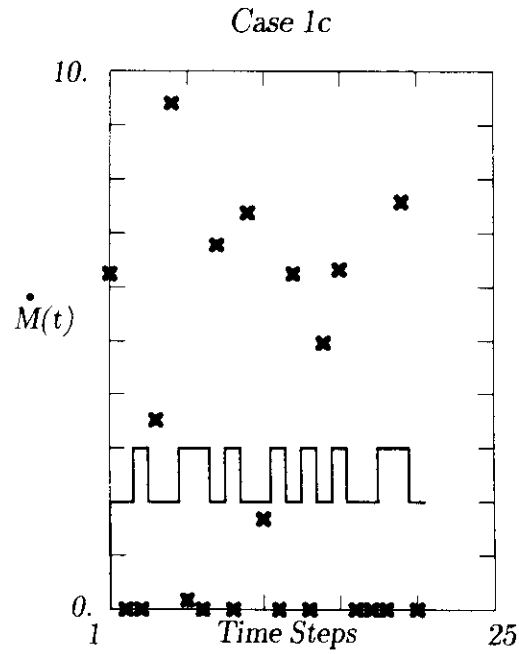

Figure 7b. Comparison of the data (solid lines) with synthetics (dashed lines) for case 1c. Notations and symbols are the same as in Figure 4.

fect, the l_1-misfit as defined by *Das and Kostrov* [1990] being 47%. However, the fit shown in Figure 7a would be considered very good for real data. Neither the moment rate distribution and history, the final moment, nor the source time function (Figure 7b) is reproduced well. The centroid in time is not far from the correct one but, as expected, the centroid along strike is not correctly obtained (see Table 1). Note also a cell rupturing well behind the rupture front. The moment was 20% larger than in the forward problem.

Case 1d: Rupture front constrained to propagate more slowly than that in forward problem, moment constrained. The solution obtained for this case using linear programming is not significantly better than for case 1c. Thus constraining the rupture front to propagate at too low a speed produced a poor fit to the data, which provides a clue that our inversion model is incorrect. We next attempt to smear out the moment distribution behind the rupture front by minimizing the maximum moment rate, as described by *Das and Kostrov* [1994], with 10% additional misfit to the data being permitted. It is found that the moment does spread out more evenly behind the rupture front but is still far from the correct solution. The results of a smoothed solution in which the sum of the modulii of the second differences of the moment rates were minimized, as formulated by *Das and Kostrov* [1994], with 10% additional misfit to the data being permitted, is very similar.

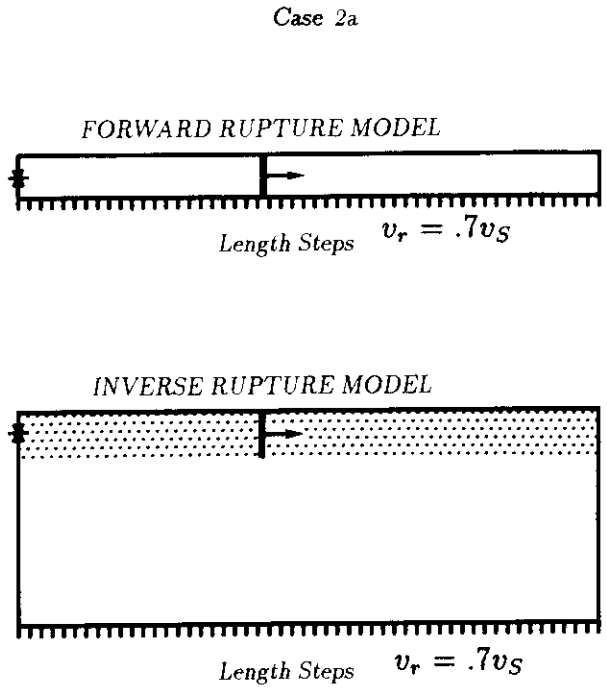

Figure 8. The forward and inverse rupture models used in case 2a. The top of the fault is at the same depth, 1 km, below the Earth's surface and the rupture nucleation points are marked by the asterisks. The shaded area in the inverse model is the part of the fault that slipped in the forward problem.

Case 2

We next consider a set of cases to obtain insight into the effect of inverting seismograms using a narrower or wider fault region than in the forward problem. We use the linear programming approach to solve the inverse problem in all cases in this section.

Case 2a: Inversion for wider fault than in forward problem. The forward and inverse rupture models for this case are illustrated in Figure 8. The forward problem is the same as in case 1, the data being shown in Figure 4, but the inverse model is taken as a 2.55 km x 250 m fault, with the top of the fault being at the same depth as in the forward case (1 km) and embedded in the same structure, $M1$. The rupture in the inversion model nucleates at the same point and propagates at the same speed ($0.7v_S$) as in the forward model, with each cell releasing moment only once as the rupture passes. The number of unknowns in this problem is 255. The only other constraint used is the positivity of moment rate. In the solution, the fit to the data is exact to three decimal places and the total moment is correctly reproduced. Figure 9a shows the moment rate history at the hypocentral depth level (stippled region in Figure 8), where the moment was released in the forward problem. Comparison with the correct solution (Figure 3) reveals that the level of moment release at the rupturing cells is not correctly obtained. Often a large moment is released at a certain cell without any moment being released at adjacent cells. No moment was released at the deeper levels even though this was allowed in the inversion. The final

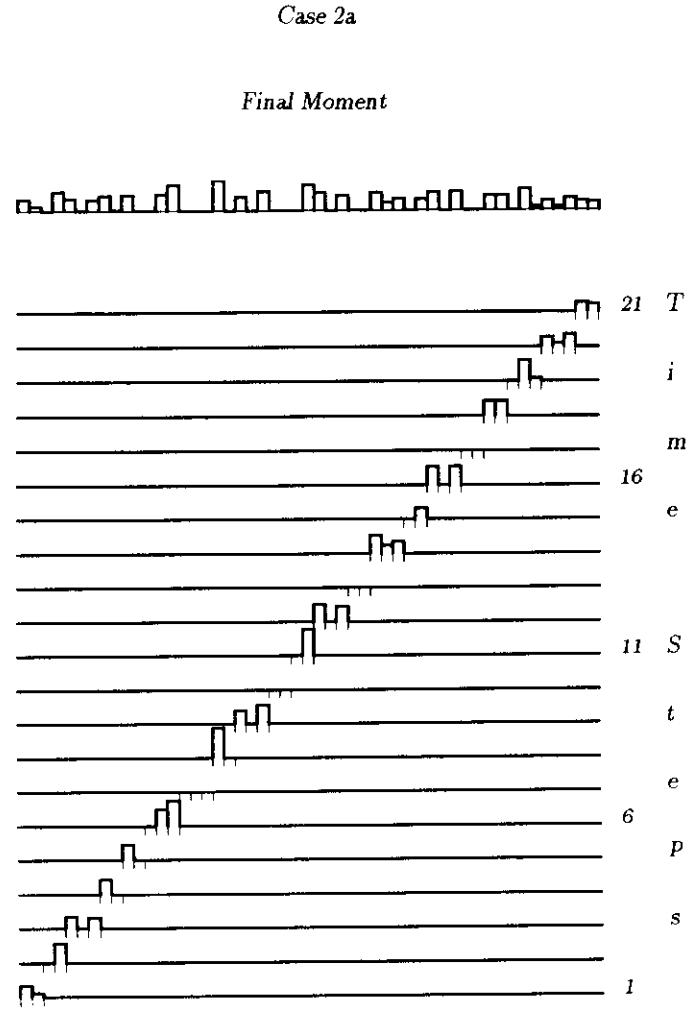

Figure 9a. Same as Figure 3 but for the inverse problem case 2a, plotted at the hypocentral cell level. Compare with Figure 3. No moment was released at the deeper parts of the fault, though this freedom was allowed in the inversion.

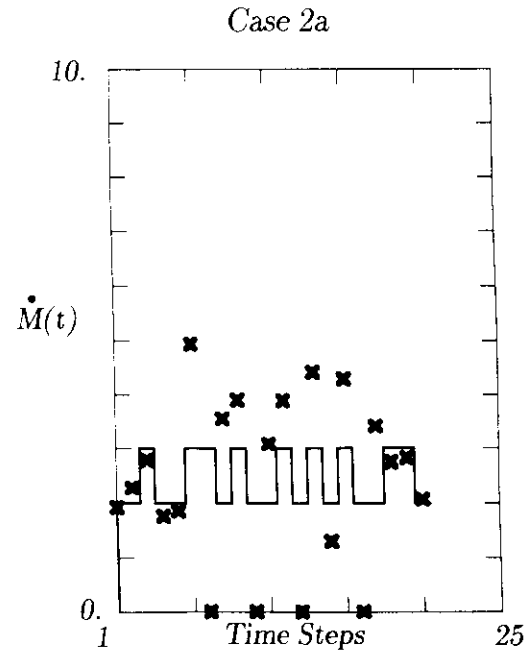

Figure 9b. Same as Figure 5a but for case 2a.

moment distribution, plotted at the top of Figure 9a, shows that the constant moment release over the fault is not reproduced. The source time function (Figure 9b) is also not reproduced correctly, but Table 1 shows that the centroids obtained are close to the correct ones. Next, the inverse problem is solved without any restriction on how often cells behind the rupture front are allowed to release moment (case 2a(2)). The number of unknowns is now 3731. The fit to the data is excellent and the total moment is correctly reproduced. The moment rate history at the hypocentral level and the final moment distribution on the fault are similar to that in case 2a. Thus when the positivity of moment rate is enforced, the width of the rupturing area and the moment centroids are correctly found, provided the rupture velocity and the Earth structure are known, even though the fault width in the inversion is larger than that used in creating the synthetic accelerograms. The moment release history, the final moment distribution, and the source time function are not, however, reproduced correctly.

Case 2b: Inversion for narrower fault area than in forward problem. The forward and inverse faulting models used in this case are illustrated in Figure 10. We construct synthetic accelerograms for the case of a 2.55 km x 250 m fault, with the rupture propagating at a constant speed of $0.7v_S$. Each cell is allowed to release moment only once as the rupture front passes. This is very similar to the classical "Haskell model" but with a curved rupture front. We perform the inversion using a 2.55 km x 50 m fault, with the top of the fault being at the same depth (1 km) as in the forward case and embedded in the same structure, $M1$. The rupture nucleation point and the rupture speed are the same in the inverse and forward models. The moment is not constrained and each cell is allowed to release moment only once as the rupture front passes. The number of unknowns in this case is 51. The l_1 misfit of the solution to the data is 18%, this difference being essentially undetectable by eye. The rupture process in time is plotted in Figure 11a. The total moment is found to be 95% of the correct value but the uniform moment release at the rupture front is not reproduced correctly; very large moment is released at certain fault cells but none at adjacent ones. The source time function, shown in Figure 11b, is not correctly reproduced. The spatial and temporal centroids of the moment distribution are found to be very close to the actual solution (Table 1). We then solve this same problem using the weak causality constraint (case 2b(2)) in order to allow more freedom in the inversion, but permit cells to release moment only once. The number of unknowns increases to 1038. The l_1 misfit is 12% and the moment is larger by about 10%. Figure 12 shows that although the rupture front position is not preassigned, the moment release is confined primarily to the vicinity of the true rupture

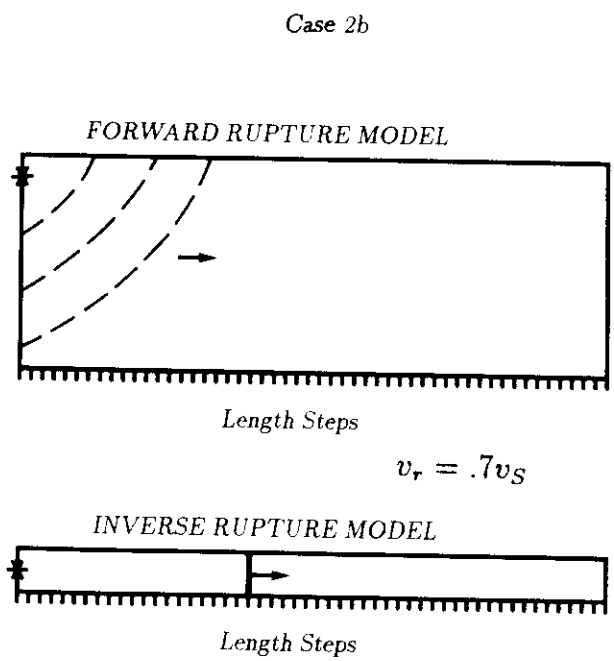

Figure 10. Same as Figure 8 but for case 2b.

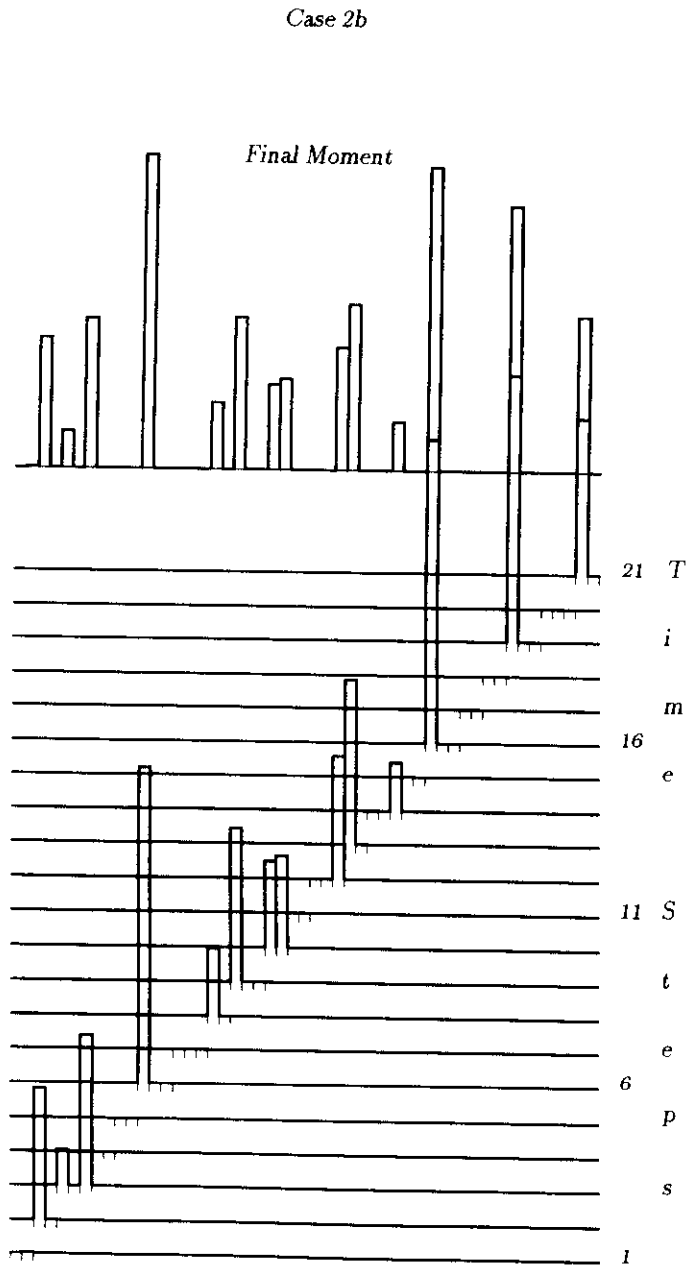

Figure 11a. Same as Figure 3 but for the inverse problem case 2b.

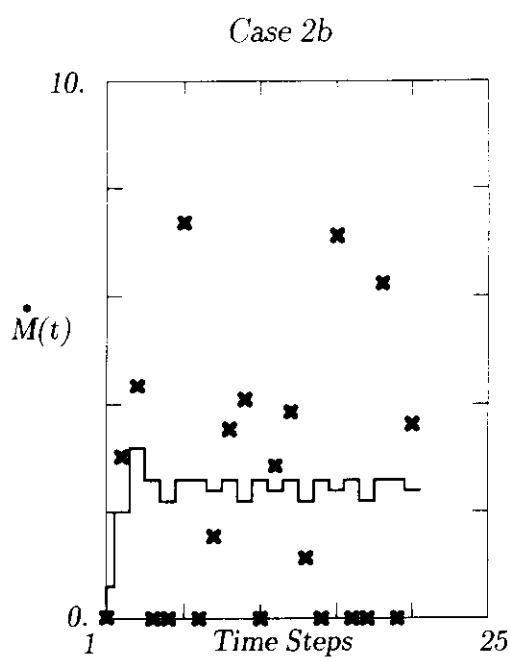

Figure 11b. Same as Figure 5a but for case 2b.

front, with some moment release both ahead and well behind it. The centroid of the moment release in both time and along fault strike is found correctly, but the source time function is not reproduced.

Case 3

We next consider a set of cases to find the effect of using incorrect Earth velocity models. Clearly, there is potential for such errors in Earth velocity to be aliased into artifacts in the solution. Here we demonstrate what some of these artifacts can be.

Case 3a: Effect of incorrect Earth structure. We construct synthetics for the 2.55 km x 50 m fault in medium $M1$, with the top of the fault located at a depth of 1 km below the Earth's surface (the forward problem of case 1). The rupture speed v_r is taken as $0.7v_S$ of medium $M1$. We solve the inverse problem using the same fault geometry but in medium $M2$. The rupture speed in the inversion is 70% of the shear wave speed of medium $M2$. Performing an SVD inversion, we obtain a very poor fit to the data with many negative moment rates. Adding constraints clearly will not improve the fit to the data. We then solve the problem using the linear programming approach and the positivity of moment rate constraint, but we are still unable to fit the data. Since the two media are different in the source region (Figure 2), we next determine the hypocentral depth in $M2$ for which the travel times of the first arrivals to the six stations are closest to those for the original source depth in $M1$, and place the fault at this depth (2.05 km) for the inversion. The forward and inverse faulting models are illustrated in Figure 13. We do not preassign the rupture speed but use only the weak causality constraint and allow grids to release moment more than once. Owing to the weak causality constraint, regions of the fault farthest from the nucleation region are found to rupture only

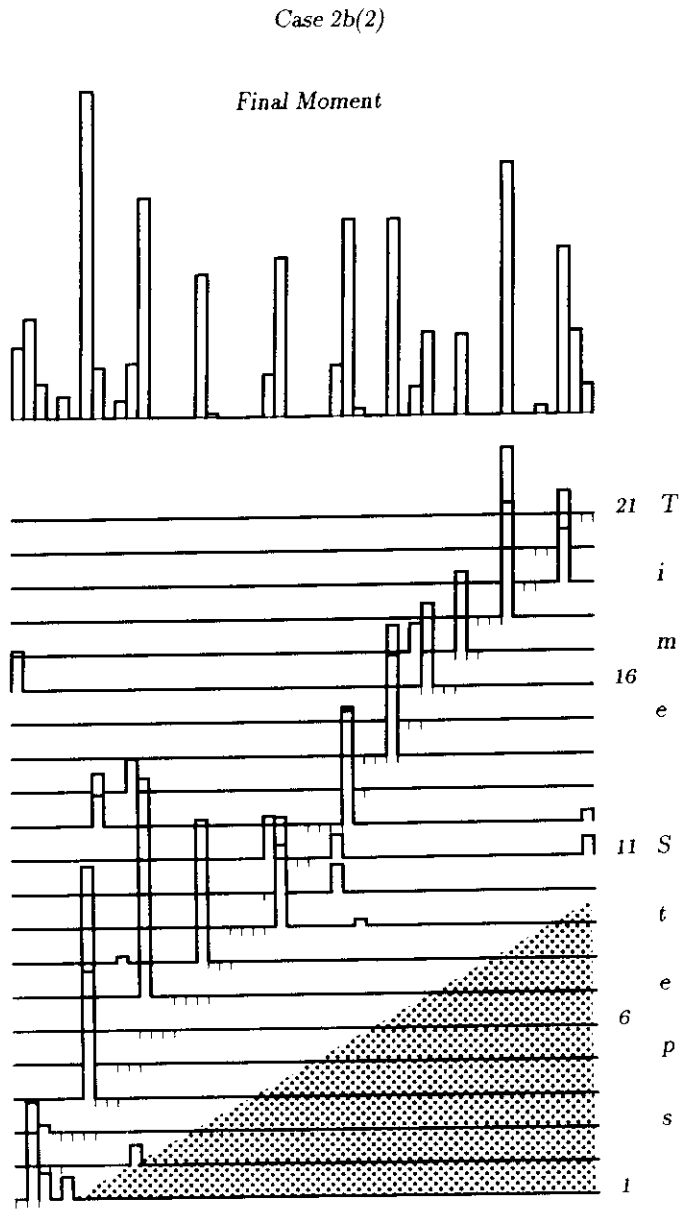

Figure 12. Same as Figure 3 but for the inverse problem case 2b(2). The tick marks shown at each time step are those for the forward problem. The region in space and time excluded by the weak causality constraint is indicated by stippling.

five time steps after nucleation, implying an apparent super P wave rupture speed. The duration of the entire source process is determined by the length of the synthetic accelerograms which is found to be 38 time steps for this inversion, the time step size being the same as in the forward problem, that is, approximately 0.1 s. The difference in the rupture durations of the forward and inverse cases is due to the different durations of the Green functions in the two media. The number of unknown moment rates is now 1818; the total moment is not constrained. Figure 14 shows the fit of the solution to the accelerograms. The fit is far from good, the l_1 norm of the misfit being 84%. Figure 15 displays the moment rate history and the final moment obtained. The first notable result is that the rupture front position is not correctly obtained and

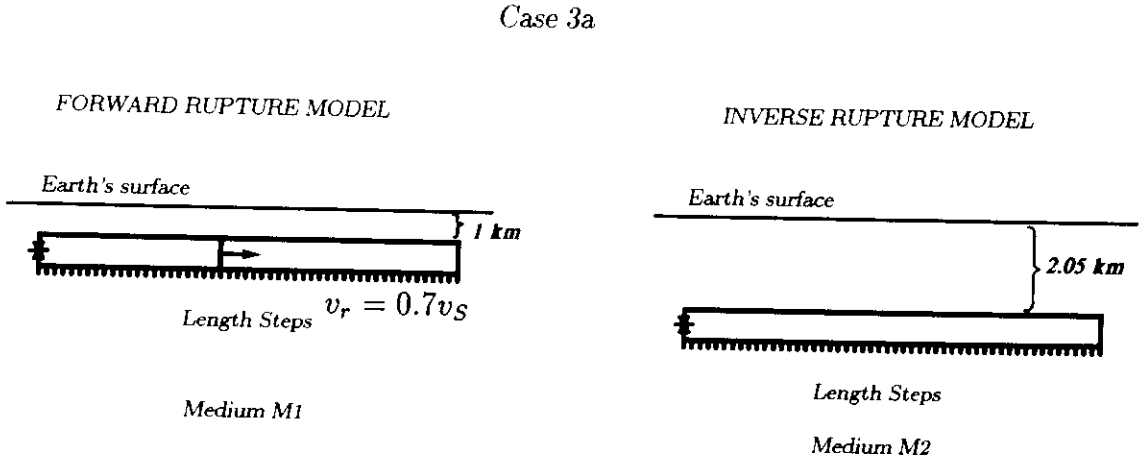

Figure 13. The forward and inverse rupture models used in case 3a. The top of the fault is at depth 1 km below the Earth's surface in the forward case and at depth 2.05 km in the inverse case. The rupture velocity in the forward problem is 70% of the shear wave speed of medium $M1$. The constraint $R2$ is used for the inversion in this case so that the rupture speed is not preassigned. The rupture nucleation points are marked by the asterisks.

the moment release appears to be somewhat randomly distributed on many parts of the fault, though an incoherent front can be identified, as indicated by the dotted line on Figure 15. The average speed of this front is about 60% of the shear wave speed of medium $M2$ at the level where the fault is located. The final uniform moment distribution of the forward problem and the source time function are not correctly reproduced. The moment obtained is 55% larger than the actual moment. The position of the centroid along strike is close to the correct one. The centroid in time, however, is far from correct which is not surprising since the duration of the process in the inversion is much longer than the correct one. But the most remarkable result here is the moment that is released at later times on the fault. Figure 15 shows an additional coherent moment release in space and time appearing from $nt = 20$ on, defining a second moment release front. We call this a "ghost front" and it illustrates how the incorrect structure manifests itself as an artifact of the solution, and would lead in the real case to being interpreted physically as a secondary rupture front. The moment release ahead of the rupture front could potentially be interpreted in the real case as evidence for super shear rupture speed and the random nature of the moment release at some other places as evidence of "asperities" rupturing. The poor fit of the synthetics to the data is the clue that our input model is incorrect.

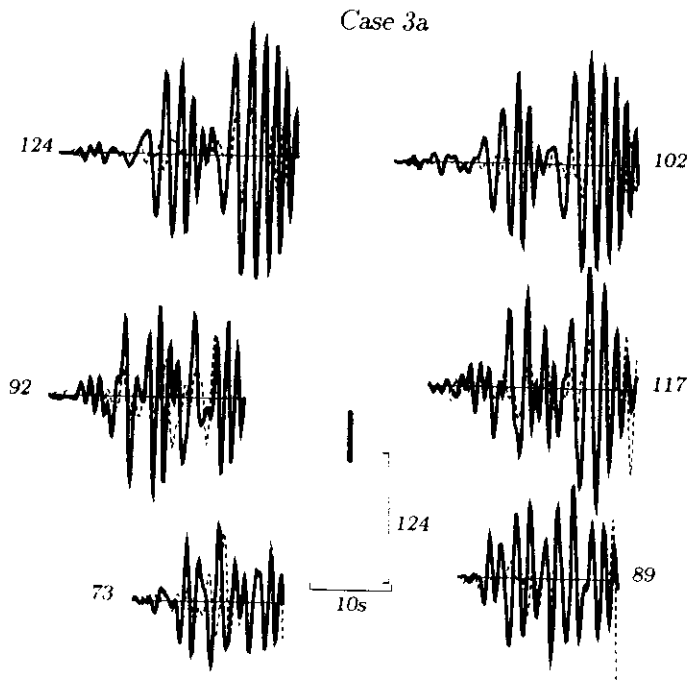

Figure 14. Same as Figure 4 but for case 3a.

Case 3b: Effect of incorrect Earth structure with a larger fault size. Finally, we use a larger fault, 2.55 km x 250 m in the inverse model, with the top of the fault located at a depth of 2.05 km, to see if this additional freedom improves the fit to the data. We find that the fit does not improve significantly. Constraining the moment only worsens the fit, as expected. Hence with the incorrect structure we are simply unable to fit the data.

Discussion and Conclusions

Using synthetic data, we solve the inverse problem for a very simple faulting model in order to gain insight into solutions of such unstable problems. We demonstrate that the constraint of positivity of moment rate on the fault is essential to reproducing all facets of the solution, namely the moment release history and distribution, the source time function, and the final moment distribution. With this constraint, we find that even if we do not preassign the rupture front position it is identifiable in the inversion, for all practical purposes, when the medium properties are known and for the simple rupture model considered here. The centroids of the moment release in space and time are generally found to be

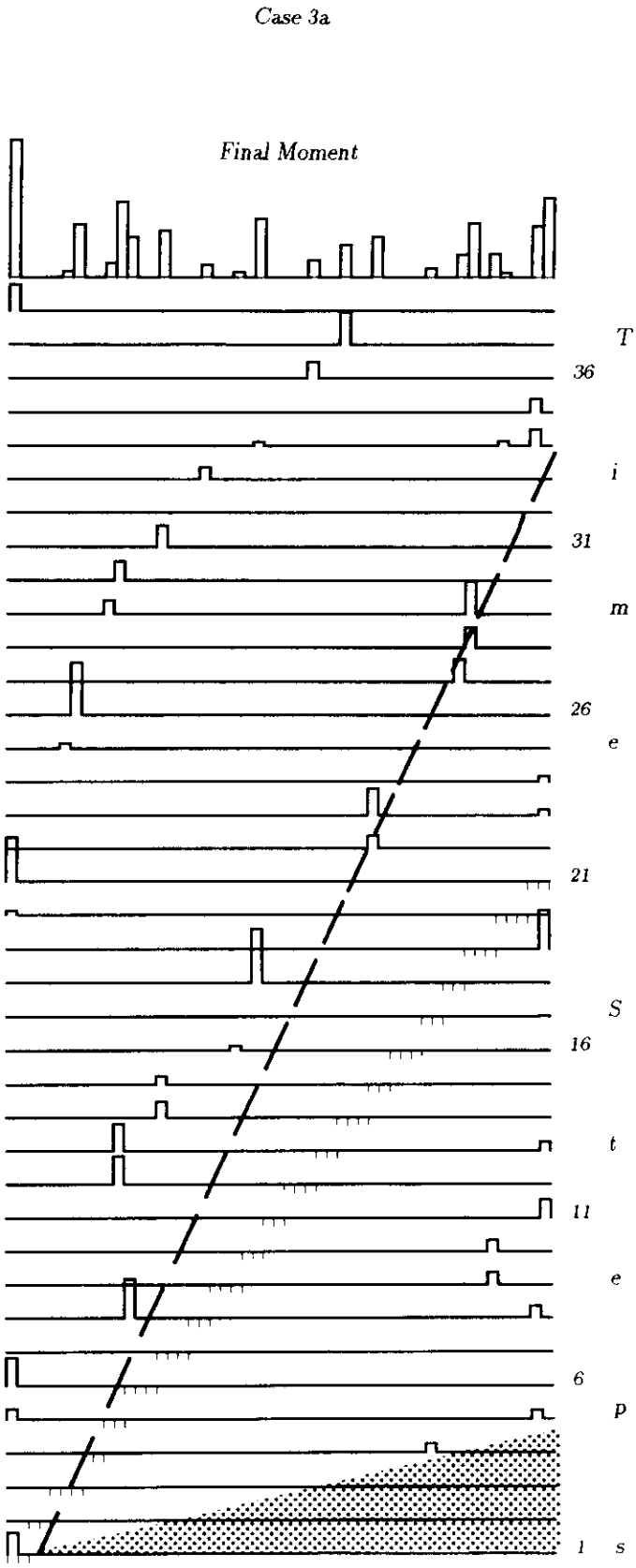

Figure 15. Same as Figure 12 but for the inverse problem case 3a. The tick marks shown at each time step are those for the forward problem in medium $M1$. The dashed line identifies the incoherent rupture front, propagating at an average speed of about 60% of the shear wave speed of the medium $M2$ at the depth where the fault is located.

close to the correct ones, even in cases where the fit to the data is poor, except that when the rupture front is constrained to propagate more slowly than in the forward problem (cases 1c and 1d), the spatial centroid is not correctly obtained. However, the constant level of moment release and the uniform final moment distribution of the forward problem generally are not correctly reproduced. In inversions of real data, such artifacts might be interpreted as evidence for heterogeneous faulting. We are unable to fit the data adequately if the rupture velocity is constrained to be lower than that in the true velocity or if the fault is constrained to be narrower than its true width. Use of incorrect crustal structure also has this effect. In the latter case, the position of the main rupture front is not obtained correctly. Instead, an additional coherent "ghost front" is obtained behind the rupture front, illustrating how poor knowledge of crustal structure can be manifest as an artifact in the solution.

The problem remains that in many cases the fit to the data is very good even when the faulting process is poorly reproduced, so that in the real case it would be difficult to know when one has obtained the correct solution. Then one must follow the suggestion of *Das and Kostrov* [1990, 1994] and consider many possible solutions, seeking physical characteristics that persist in many solutions. For example, if solutions resulting from differing constraints all show that the main moment release was at a particular region of the fault or give nearly the same average rupture velocity, then we may have some confidence in these features of the solution. Using data from the 1989 Macquarie Ridge earthquake, *Das and Kostrov* [1994] showed how to perform further optimizations to see if a particular common feature persists. If it does, then can one have some confidence that it is truly representative of the actual faulting process. This study, using artificial, noise-free data, also shows that small variations in the quantities obtained, such as rupture velocity, moment release over the fault, and so on, may not be reliable. The complications in using real, noisy data, deconvolution of instrument responses, and so on, will only make the situation even more difficult.

The results presented here suggest that it is essential to carry out a study such as this before inverting real data in order to have some idea of the limitations of the inversion for the particular case under investigation.

Acknowledgments. This study was started while one of the authors (P.S.) visited the Department of Earth Sciences in Oxford in the framework of agreements between the Royal Society and Accademia Nazionale dei Lincei, and was continued under partial support from the EC program, Environment and Climate, Topic IV.1.1, Natural Risks – Seismic Hazard, under EPOCH contract EPOC-CT91-0042 and ENVIRONMENT contract EN5V-CT94-0513. We would like to thank Steve Hartzell and Bill Foxall, and the anonymous Associate Editor for very thorough reviews and the many constructive comments that helped to improve and clarify the manuscript. We would also like to thank B. V. Kostrov for many helpful suggestions and comments during the entire course of this work. The computations were done on the Cray-YMP8 at the Rutherford-Appleton Laboratories, Didcot, U.K. under a Supercomputing grant obtained through the Natural Environmental Research Council of the U. K.

References

Aki, K., and P. G. Richards, *Quantitative Seismology: Theory and Methods*, 932 pp., W.H. Freeman, New York, 1980.

Ben-Menahem, A., and D. G. Harkrider, Radiation patterns of seismic surface waves from buried dipolar point sources in a flat stratified Earth, *J.Geophys. Res., 69*, 2605-2620, 1964.

Backus, G. E., Comparing hard and soft prior bounds in geophysical inverse problems, *Geophys. J., 94*, 249-261, 1988.

Beroza, G. C., and P. Spudich, Linearized inversion of fault rupture behavior: Application to the 1984 Morgan Hill, California earthquake, *J. Geophys. Res., 93*, 6275-6296, 1988.

Das, S., Tectonic implications of the moment distribution of the 1986 Andreanof Islands earthquake, paper presented at the *International Symposium of Earthquake Source Physics and Earthquake Precursors*, pp. 143-146; sponsored by IASPEI, NCSPEI, SCJ and SSJ, Univ. Tokyo, Tokyo, Japan, 19-22 Nov, 1990.

Das, S., and B. V. Kostrov, Inversion for seismic slip rate and distribution with stabilizing constraints: Application to the 1986 Andreanof Islands earthquake, *J. Geophys. Res., 95*, 6899-6913, 1990.

Das, S., and B. V. Kostrov, Diversity of solutions of the problem of earthquake faulting inversion. Application to SH waves for the great 1989 Macquarie Ridge earthquake, *Phys. Earth Planet. Inter., 85*, 293-318, 1994.

Das, S., P. Suhadolc and B. V. Kostrov, Realistic inversions to obtain gross properties of the earthquake faulting process, *Tectonophysics*, in press, 1995.

Florsch, N., D. Faeh, P. Suhadolc, and G. F. Panza, Complete synthetic seismograms for high-frequency multimode SH waves, edited by A. Udias and E. Buforn, *Proc. El Escorial Workshop, Pure Appl. Geophys, 136*, 529-560, 1991.

Harkrider, D. G., Surface waves in multilayered elastic media, 1, Rayleigh and Love waves from buried sources in a multilayered elastic half-space, *Bull. Seismol. Soc. Am., 54*, 627-679, 1964.

Hartzell, S. H., and T. H. Heaton, Inversion of strong-ground motion and teleseismic waveform data for the fault rupture history of the 1979 Imperial Valley, California earthquake, *Bull. Seismol. Soc. Am., 73*, 1553-1583, 1983.

Hartzell, S. H., and P. Liu, Calculation of earthquake rupture histories using a hybrid global search algorithm: Application to the 1992 Landers, California earthquake, *Phys. Earth Planet. Inter.*, in press, 1995.

Hartzell, S., G. S. Stewart, and C. Mendoza, Comparison of L_1 and L_2 norms in a teleseismic waveform inversion for the slip history of the Loma Prieta, California, earthquake, *Bull. Seism. Soc. Am., 81*, 1518-1539, 1991.

Haskell, N. A., Total energy spectral density of elastic wave radiation from propagating faults, *Bull. Seismol. Soc. Am., 54*, 1811-1841, 1964.

Haskell, N. A., Total energy and energy spectral density of elastic wave radiation from propagating faults, II, A statistical source model, *Bull. Seismol. Soc. Am., 56*, 125-140, 1966.

Haskell, N. A., Elastic displacements in the near-field of a propagating fault, *Bull. Seismol. Soc. Am., 59*, 865-908, 1969.

Jackson, D., The use of a priori data to resolve non-uniqueness in linear inversion, *Geophys. J. R. Astron. Soc., 57*, 137-158, 1979.

Kikuchi, M., and Y. Fukao, Iterative deconvolution of complex body waves from great earthquakes – The Tokachi-Oki earthquake of 1968, *Phys. Earth Planet. Inter., 37*, 235-248, 1985.

Kikuchi, M., and H. Kanamori, Inversion of the complex body waves, *Bull. Seismol. Soc. Am., 72*, 491-506, 1982.

Kostrov, B. V., The theory of the focus for tectonic earthquakes, *Izv. Earth Phys.*, 258-267, 1970.

Kostrov, B. V., Mechanics of the Tectonic Earthquake Focus (in Russion), 176 pp., Nauka, Moscow, USSR, 1975.

Kostrov, B. V., and S. Das, Principles of earthquake source mechanics, *Appl. Math. Mech. Ser.*, 286 pp., Cambridge University Press, New York, 1988.

Madariaga, R., The dynamic field of Haskell's rectangular dislocation fault model, *Bull. Seismol. Soc. Am., 68*, 869-887, 1978.

Mendoza, C., and S. H. Hartzell, Aftershock patterns and main shock faulting, *Bull. Seismol. Soc. Am., 78*, 1438-1449, 1988a.

Mendoza, C., and S. H. Hartzell, Inversion for slip distribution using teleseismic P waveforms: North Palm Springs, Borah Peak, and Michoacan earthquakes, *Bull. Seismol. Soc. Am., 78*, 1092-1111, 1988b.

Mendoza, C., and S. H. Hartzell, Slip distribution of the 19 September 1985 Michoacan, Mexico, earthquake: Near-source and teleseismic constraints, *Bull Seismol. Soc. Am., 79*, 655-669, 1989.

Miyatake, T., Reconstruction of dynamic rupture process of an earthquake with constraints of kinematic parameters, *Geophys. Res. Lett., 19*, 349-352, 1992.

Olson, A. H., and J. G. Anderson, Implications of frequency-domain inversion of earthquake ground motions for resolving the space-time dependence of slip on an extended fault, *Geophys. J., 94*, 443-455, 1988.

Olson, A. H., and R. J. Apsel, Finite faults and inverse theory with applications to the 1979 Imperial Valley earthquake, *Bull. Seismol. Soc. Am., 72*, 1969-2001, 1982.

Panza, G. F., Synthetic seismograms: The Rayleigh waves modal summation, *J. Geophys., 58*, 125-145, 1985.

Panza, G. F., and P. Suhadolc, Complete strong motion synthetics, *Seismic Strong Motion Synthetics, Computational Techniques*, editied by B. A. Bolt, vol. 4, pp. 153-204, Academic, San Diego, Calif., 1987.

Parker, R. L., Geophysical Inverse Theory, 386pp., Princeton Univ. Press, Princeton, New Jersey, 1994.

Press, W. H., B. P. Flannery, S. A. Teukolsky, and W. T. Vetterling, *Numerical recipes: The Art of Scientific Computing*, 818 pp., Cambridge University Press, New York, 1986.

Ruff, L. J., Fault asperities inferred from seismic body waves, in *Earthquakes: Observation, theory and interpretation*, edited by H. Kanamori and E. Boschi, pp. 251-276, North-Holland, New York, 1983.

Suhadolc, P., P. Harabglia and G. F. Panza, Deterministic modeling and estimate of strong ground motion: The Iripinia, Italy, November 23, 1980 earthquake, *Proc. 9th Euro. Conf. on Earthquake Engg.*, Kucherenko Tsniisk USSR Gosstroy, Moscow, 100-109, 1990.

Tarantola, A., Inverse problem theory. Methods for data fitting and model parameter estimation, 613pp., Elsevier, Amsterdam, 1987.

S. Das, University of Oxford, Department of Earth Sciences, Parks Road, Oxford OX1 3PR, U. K. (e-mail:das@earth.ox.ac.uk)

P. Suhadolc, Universita di Trieste, Istituto di Geodesia e Geofisica, Via E. Weiss, 4, 34127 Trieste, Italy. (e-mail: suhadolc@geosun0.univ.trieste.it)

(Received February 6, 1995; revised November 10, 1995; accepted November 17, 1995.)

Realistic inversions to obtain gross properties of the earthquake faulting process [1]

S. Das

Department of Earth Sciences, University of Oxford, Parks Road, Oxford OX1 3PR, UK.

P. Suhadolc

Istituto di Geodesia e Geofisica, Universita di Trieste, Trieste, Italy

B. V. Kostrov

Institute of Physics of the Earth, B. Gruzinskaya 10, Moscow D242, Russia.

Abstract

The problem is to find if we are able to determine correctly the average properties of the actual earthquake faulting process, which occurs in reality in the Earth at microscopic scales, from a solution of a feasible inverse problem. In order to investigate this, we use synthetic accelerograms constructed in the vicinity of a 20km $\times$ 5km dipping thrust fault for a discrete analog of the Haskell-type of fault model as the data and perform the inversion using much coarser spatial and temporal grids than used in constructing the data and widely used inversion methods. We show that we are essentially unable to obtain the proper (known) results when we use a least-squares (Singular Value Decomposition) method due to the fact that many negative values of moment rate, which did not exist in the forward problem, are produced though the data are well fit. Inversions using the SVD method together with smoothing constraints or exclusion of small singular values yield an improved solution but the actual values to be used must be obtained by trial-and-error and do not contribute to our insight as to how to solve the problem with real data. Finally, we show that if we enforce the condition that

[1] *Tectonophysics* Special issue entitled Seismic Source Parameters: from Microearthquakes to Large Events, in press.

there are no negative moment rates, using in this case the method of linear programming, we are able to reproduce many aspects of the original solution better.

Introduction

In order to investigate the possiblity of inverting seismograms to obtain correctly the details of the rupturing process, Das and Suhadolc (1995) set up an experiment using artificial data for a simple faulting model and widely used standard inversion methods. Synthetic accelerograms were constructed in the vicinity of an earthquake for the discrete analog of the Haskell-type rupture model with a prescribed rupture velocity in a layered medium and with a constant level of moment being released once by each cell as the rupture front passed by. It was shown that it is generally possible to correctly invert for many aspects of the rupture process provided physically based constraints are used to stabilize the inverse problem. This was shown to be so except in special cases where the source crustal structure is poorly known or when the rupture area in the inversion is constrained to be smaller then the actual fault area. In that study, referred to as Paper I from here on, the spatial and temporal grid sizes used in the inversion were the same in the inverse as in the forward problem. In reality, the actual scales at which the rupture propagation takes place in the Earth is microscopic whereas the inverse problem must be solved using finite grids. Therefore, it is important to study whether the inverse solution obtained gives us a picture of the actual solution averaged over the larger grid. In this paper, we therefore consider the problem where the synthetic accelerograms used as "data" are constructed using very fine grids but the inversion is performed using much coarser grids. For this, the wavelengths of the waves used in the inversion must be consistent with the grid sizes used. In addition, the fault discretization itself is a stabilizing factor but may not necessarily lead to the correct solution.

The problem

Since the details of the problem description, the construction of the synthetic accelerograms and the method of inversion, together with a complete reference list and discussion of related studies of fault rupture process inversion, were given in Paper I, we only briefly describe the main points of the problem set-up here. As in Paper I, we again consider a discrete analog of the Haskell-type of dislocation which propagates from the hypocenter at the prescribed velocity of about 70% of the shear wave speed of the layer and covers a given rectangular area. The fault area is divided into square cells and the source time function into steps. A constant level of moment is released at the time of rupture of a cell and with each cell releasing moment during only one time step as the rupture passes it. The fault geometry and station distribution are shown in Figure 1 and is the same as in Paper I except that here we use a much larger fault of size 20km x 5km, with the top of the fault being located at the deeper level of 5km below the Earth's surface. We generate the synthetic accelerograms using fine cells of size 156.25m (=20km/128, where the fault is 20km long and it has 128 cells along its length; there are 32 cells along its width). The temporal step size is taken as .1s (200/2048=.097..s, to be exact) and the Green functions are computed for a maximum frequency of 1 Hz. The crustal wave velocities used are shown in Figure 2. To obtain the Green functions for the larger cells necessary for the inversions, we simply average over the appropriate number of spatial cells. When the larger spatial cells are used, we also average the Green functions over the appropriate number of temporal steps to have temporal and spatial discretizations that are consistent with one another.

Choice of cell size for the inversion

We need to decide how large the cells in the inversion should be. Clearly, the smaller the cells the better the approximation to the integral equation being solved but the larger the number of unknowns. In order to make this decision, we consider spatial cells which are two, four and eight times larger than that used in the forward problem and construct the synthetic

accelerograms with the corresponding Green functions to see how different they are from those constructed with fine discretization of the fault. Figure 3 shows the synthetic accelerograms, constructed using the finest cells and that obtained using 8 times larger spatial cells and 4 times larger temporal steps. The l_1, l_2 and l_∞ norms of the differences between these two sets of synthetic data are 23%, 27% and 30%, respectively, though the difference are barely visible visually. These numbers are much smaller for the other smaller cell and time step sizes tested. For the fault under study, use of this cell size would mean 64 spatial cells and 26 time steps, that is, a maximum of 1664 unknowns. In particular cases studied, the number of unknowns may be smaller as cells are excluded by causality or other considerations. It would be difficult to have too many more unknowns, and hence smaller cells, because as the approximation to the integral equation improves by going to smaller and smaller cells, the condition number of the matrix increases making the problem more and more unstable. We shall use this coarseness of cell for all the inversions in this study. The discussion of the use of finitely sampled data to infer some continuous property, of the Earth say, was discussed by Backus and Gilbert (1967, 1968) in a set of now-classic papers. As pointed out by Backus and Gilbert (1967), since the amount of data is finite, the problem of finding a continuous function from it is indeterminate. In other words, the stability of the system of equations decreases (that is, the condition number of the matrix A increases) as we use finer and finer discretization of the fault for the inversion.

In Paper I, we showed that minimum norm solutions and solutions which are smoothed in some sense, say the solution with the smallest first or second differences in space and time, did not reproduce all aspects of the solution, though the position of the rupture front was approximately found. On the other hand, we showed that physically based constraints such as disallowing back slip to occur on the fault reproduced the solution better. In Paper I we used the same size cell and time step size in the inversion as in constructing the synthetic data.

In this paper, we investigate how well we can infer the moment rate history and distribution due to a rupturing fault when the inverse problem is solved using much coarser spatial and temporal discretization than used in generating the synthetic accelerograms. Figure 4 shows the entire time history of moment release used in the forward problem for fine cells and time steps but plotted averaged over the coarse cells and time steps to present the picture with which the results of the inversion must be compared. Note that in the discrete representation of the forward model the rupture front, which is obtained by discretizing the constant speed rupture front, is in fact quite non-uniform. It may also be pointed out that because of the roughness of the gridding on the fault, the strong singularities at the fault edges, which exist in the classical Haskell model, are not present in the forward models used in this paper.

Results

More than 30 inversions were performed for this study. Table 1 summarises the cases which will be discussed in detail in the paper and the results. Simply as a test, we first solve the problem $A\mathbf{x} = \mathbf{b}$ using the synthetic data $\mathbf{b}$ generated with the same coarse cell and time step as for the inverse problem. The rupture front is pre-assigned to the known front for this test and each cell is allowed to release moment only once in the inversion, as in the forward problem. The number of unknown x's is 177. A least-squares solution performed using the Singular Value Decomposition (SVD) method agreed with the input to several decimal places, thus testing the setting up of the matrix system and the computer program used. Before replacing the r.h.s $\mathbf{b}$ by the seismogram obtained using the fine cells, we perform some tests to see how well the rupture front is identifiable when the problem is solved without constraining the rupture front. This is similar to some of the cases discussed in Paper I for the short fault but since the stability of the problem can change for the larger fault, it is useful to perform this investigation here.

We relax the requirement that the rupture front is preassigned to the actual front and

instead allow all cells behind the S-wave front from the hypocentral cell to slip during the entire source process. The causal front is thus only a little larger than the rupture front of the forward problem which propagated at about 70% of the S-wave velocity, but the number of cells permitted to slip behind the front is large. The number of unknowns is now 1160. Applying the SVD method, we find that the rupture front is clearly identifiable in the solution but the moment rates obtained contain some negative moment values. The source time function and the final moment on the fault are shown in Figures 5 and 6, respectively. Figure 5 shows that the source time function agrees very well with the input and the final moment (area under this curve), which was not set a priori, is correct. The negative values of the moment rate, though small, have a significant effect on the final moment distribution over the fault, which is seen in Figure 6 to have large deviations around the correct moment level released at each cell in the forward problem. The spatial and temporal centroid obtained by the solution agrees well with that for the forward problem. By excluding some of the smaller singular values the solution can be improved significantly. For example, if we exclude singular values which are less than .01% of the largest singular value, we obtain the final moment distribution on the fault as shown in Figure 7. However, the number of singular values that have to be excluded to improve the solution can only be found by trial-and-error and thus only when the expected answer is known, making this a not very useful exercise as it gives little insight into how to solve the problem with real data. Constraining the rupture front even less, that is by the P-wave front or using the "weak-causality" condition (defined in Paper I and in Das and Kostrov (1990)) only makes the solution even further from the input.

We now continue the study by using for the r.h.s b the seismogram for fine gridding (the solid lines in Figure 3), the case which is the focus of this study. The results obtained above suggests that we should not expect satisfactory results and indeed we shall show that using the least-squares (SVD) method this is so. We preassign the rupture front to the known front,

and allow each cell to release moment only once in the inversion, as in the forward problem, resulting in 177 unknown x's in the problem. The solution had many negative values for the moment rate, though the fit to the data is excellent (since the differences are not seen visually, they are not plotted here). Again, as before, excluding some of the smaller singular values does improve the solution. Excluding too many or too few singular values made the solution worse.

We next constrained the moment, setting it to be equal to the known moment of the forward problem and re-solved the problem. This is referred to as Case A in Table 1. The time history of moment rate release over the fault is plotted in Figure 8 and shows that there are again many negative values. The final moment oscillates around the known input value and the source time function also oscillates around the known input, but has no negative values (not shown). As in the previous case selectively excluding singular values did improve the solution.

Next, we search for the solution which has the smoothest first differences in space and time to see if such a smoothed solution better fits the input. For this, we minimise the square of the residual (Ax-b) together with the squares of the first differences of x in two space dimensions and in time. The second term is multiplied by a weighting factor, and the size of the weight is varied. Weights of .1, .2, .5, 1., 2., 2.5, 4.,and 8. were used. We find that as this weight was increased, that is, the solution was made smoother, the negative moment rates became fewer and smaller. We refer to the case with weight = 4. as Case B in Table 1. The source time function obtained is shown in Figure 9, compared with that for the forward problem. The moment rate agrees with that for the input for the first few time steps but then overshoots it and oscillates about it. The moment rate release history over the fault visually looks similar to that for the forward problem, shown in Figure 4 and is therefore not plotted, but the actual values do not agree well with the proper solution. The final moment

distribution over the fault has some (as large as ±50 percent in some places) deviations from the proper constant value over the fault. So smoothing the first differences does make the negative values of moment rate obtained fewer and smaller, but the solution does not become closer to the actual solution.

The inverse problem can be formulated in terms of slip or slip rate (see Paper I) with the use of the appropriate kernel in the integral equation, and in the above we used the formulation in terms of the slip rates. We next checked if solving the problem in terms of the slip improved the situation. From a mathematical point of view there should of course be no difference but we test if there is any difference computationally. We repeated the entire set of cases discussed above but no aspect of the solution improved.

Next, we preassign the rupture front in the inversion to the known rupture front and test if we are able to find the rupture front in the case when coarse cells are used in the inversion and the fine cell synthetic data is used. The rupture front is constrained to move at the known rupture speed of about $.7v_s$, but all cells behind the front are now allowed to slip as often as necessary. The number of unknowns increases to 923. This case is referred to as Case C in Table 1 and the entire moment rate release time history over the fault is plotted in Figure 10, the moment rate function is shown in Figure 11 and the final moment in Figure 12. Figure 10 shows that when cells behind the rupture front are not restrained from slipping, they do slip and release non-negligible amount of moment. This figure also shows that at the end of the process the entire fault is still slipping in the inversion whereas in the forward problem the entire fault has come to a rest. Figure 11 shows that the moment rate history is reproduced very poorly and Figure 12 shows that the final moment, which is distributed uniformly over the fault in the forward problem, is quite uneven in the inversion. As before, by smoothing the first derivative the result improves in that the solution has less and smaller negative values for moment rate, and excluding some singular values selectively, say, excluding relatively small

ones also has the same effect but in both cases the actual solution, though nearly positive, does not closely resemble the input. Constraining the rupture to move at about the shear wave velocity increases the number of unknowns to 1160 and again the solution is poor.

Thus we are clearly unable to reproduce the solution when we perform the inversion with much coarser cells than those with which the synthetic data were generated. We next filter the fine cell x and the coarse cell A, that is the fine data and the coarse Green functions, with the same filter parameters and using the filtered x and A perform the inversion using the SVD method to see how well we are able to reproduce the input. Even for the case when the rupture front is preassigned to the actual front and each cell is allowed to slip only once, all aspects of the solution are poorly reproduced. As before, the solution can be improved by excluding small singular values, but again this does not teach us how to solve the real problem. Solving the problem by allowing all cells behind the front to slip more than once does not improve the solution, neither does constraining the rupture front by the P or the S wave front.

Finally, we solve the problems discussed above with the additional constraint that the moment rates are constrained to be positive by applying the method of linear programming developed by Das and Kostrov (1990, 1994) for this problem. As before, the moment is constrained to the known value. We first solve the problem when the rupture front is preassigned and each cell slips only once in time (177 unknowns). This case is labelled Case D in Table 1. All aspects of the solution (that is, time history of moment rate distribution, source time function and final moment distribution on fault) are the same as the input for all practical purposes and are not plotted since the minor differences are not seen visually.

Next, we perform the inversion preassigning the rupture front to move at the known speed but allow all cells behind the front to slip as often as necessary. The number of unknown is 923. This case is labelled Case E in Table 1. The complete moment release history is shown

in Figure 13. The moment release pattern over the fault in time is reproduced correctly for all practical purposes, with occasionally an additional cell behind the actual rupture front and adjacent to it also having some small moment release. Figure 13 shows that are also a few instances where a small amount of moment is released well behind the actual rupture front, which is not present in the correct solution. At the final time step, the entire fault is at rest as in the forward problem, and a feature we were unable to reproduce in the analogous Case C. We also reproduce the final moment and the source time function correctly.

Finally, we consider the case when the rupture front is allowed to be larger than the actual front and limit it by the S-wave front in Case F and by the P-wave front in Case G. We find that as long as the moment rates are constrained to be positive, we again are able to reproduce the solution properly. The complete moment release history is shown for Case F in Figure 14, with behaviour similar to that described for Case E (Figure 13).

Discussion and Conclusions

In order to test if it is possible to invert seismograms to obtain correctly the details of the rupturing process, we perform more than 30 inversions using well known inversion techniques and synthetic accelerograms for the discrete analog of the Haskell-type of rupture propagating at a prescribed velocity and releasing a constant level of moment only once at the rupture front. We show that unless the positiveness of slip rate or moment rate is enforced, the expected solution is not reproduced. A least-squares solution produces many large negative values of the moment rates. Trying to then reduce these negative values by smoothing the first differences, say, or excluding some of the smaller singular values of the linear system does reduce the negative values but does not necessarily bring it closer to the actual solution. In any case, since the improvement in the solution depends on the weighting factor used in the smoothing or the number of singular values excluded, this teaches us nothing about how to solve the real problem. Enforcing the "no back-slip" constraint , that is, disallowing negative

moment rates, however does produce the proper results.

In this paper, the positiveness of moment rates was enforced using the method of linear programming. Clearly, other methods of enforcing this constraint may be equally acceptable, though we have not tested other such techniques for this paper, as our goal here is simply to demonstrate that this constraint is essential. Such an alternative method has been used for this problem by Hartzell and Heaton (1983) and applied by Hartzell and Liu (1995), by Hartzell et al. (1991) and by Wald and Heaton (1994), to mention only a few such applications. Hartzell and Heaton (1983) showed that using small subfaults and then smoothing the solution, in addition to imposing the positivity constraint, may be desirable.

Finally, we discuss the limitations of this study due to the use of a very simple forward model of the faulting process. Clearly, all our negative conclusions, say the fact that we are unable to reproduce the correct solution without the positivity constraint, will hold for more complex cases. On the other hand, our positive conclusions, for example, that we can reproduce the rupture front position correctly by using the positivity constraint, as in Cases F and G, is only applicable to the case studied here. This paper demonstrates the difficulties we encounter even in the simple case of a Haskell-type faulting model. Clearly more realistic models like crack models with more variable rupture propagation speeds would present even greater difficulties and the current approach of solving the inverse problem used here may not even be usable.

Acknowledgements

This study was partially supported by EC program, Environment and Climate, Topic IV.1.1, Natural Risks – Seismic Hazard, under the EPOCH contract EPOC-CT91-0042 and the ENVIRONMENT contract EN5V-CT94-0513. The computations were done on the Cray-YMP8 at the Rutherford-Appleton Laboratories, Didcot, UK under a Supercomputing grant obtained through the Natural Environmental Research Council of the U. K. We would like to thank Steve Hartzell and an anonymous reviewer for encouraging reviews.

References

Backus, G. and Gilbert, F., 1967. Numerical applications of a formalism for geophysical inverse problems, Geophys. J. Roy. Astron. Soc., 13:247-276.

Backus, G. and Gilbert, F., 1968. The resolving power of gross earth data, Geophys. J. Roy. Astron. Soc., 16:169-205.

Das, S. and Kostrov, B.V., 1990. Inversion for seismic slip rate and distribution with stabilizing constraints: Application to the 1986 Andreanof Islands earthquake, J. Geophys. Res., 95:6899-6913.

Das, S. and Kostrov, B.V., 1994. Diversity of solutions of the problem of earthquake faulting inversion. Application to SH waves for the great 1989 Macquarie Ridge earthquake, Phys. Earth Planet. Int., 85:293-318.

Das, S. and Suhadolc, P., 1995. On the inverse problem for earthquake rupture. The Haskell-type source model, J. Geophys. Res., submitted.

Hartzell, S.H. and Heaton, T.H., 1983. Inversion of strong-ground motion and teleseismic waveform data for the fault rupture history of the 1979 Imperial Valley, California earthquake, Bull. Seismol. Soc. Am., 73:1553-1583.

Hartzell, S. and Liu, P., 1995. Calculation of earthquake rupture histories using a hybrid global search algorithm: Application to the 1992 Landers, California earthquake, Phys. Earth

Planet. Int., in press.

Hartzell, S., Stewart, G. S. and C. Mendoza, 1991. Comparison of L_1 and L_2 norms in a teleseismic waveform inversion for the slip history of the Loma Prieta, California, earthquake, Bull. Seism. Soc. Am., 81:1518-1539.

Wald, D. J. and Heaton, T. H., 1994. Spatial and temporal distribution of slip for the 1992 Landers, California, earthquake, Bull. Seism. Soc. Am., 84:668-691.

Figure Captions

Figure 1. Fault and station geometry used in this study, shown in plane view and fault geometry is cross-section. The star denotes the hypocenter.

Figure 2. The P- and S-wave velocity profiles with depth in the crust for the medium used in this study.

Figure 3. Synthetic accelerograms constructed using the spatial cells of size 156.25m and temporal steps of .1s are shown by the solid line. Synthetic accelerograms using 8 times larger spatial (1.25km) and 4 times larger temporal steps (.4s) are shown by the dashed line.

Figure 4. The entire time history of the moment release on the fault used in the forward problem using fine cells but plotted here averaged over the coarse cells. Figures 8, 10, 13 and 14 for the solution must be compared with this figure.

Figure 5. Moment rate versus time for the forward problem (solid line) and for inversion (crosses) for the coarse cell Green functions and accelerograms when the rupture is constarined by the S-wave front and all cells behind it allowed to slip as often as necessary using the SVD method.

Figure 6. Final moment distribution for the forward problem (thick solid line) compared

with the same inversion (thin solid line) as in Figure 5. The final moment is against the fault length for the four cells along fault width, nh=1 indicating the shallowest cell level and nh=4 the deepest.

Figure 7. Same as Figure 6 but for the inversion in which singular values which are less than .01% of the largest singular value are excluded.

Figure 8. The entire time history of the moment release on the fault for Case A, plotted at the same scale as Figure 4. Compare with Figure 4.

Figure 9. Same as Figure 5 but for Case B.

Figure 10. Same as Figure 8 but for Case C. Compare with Figure 4.

Figure 11. Same as Figure 5 but for Case C.

Figure 12. Same as Figure 6 but for Case C.

Figure 13. Same as Figure 8 but for Case E. Compare with Figure 4.

Figure 14. Same as Figure 8 but for Case F. Compare with Figure 4.

TABLE 1. INVERSION PARAMETERS AND RESULTS

Case	Constraints	Solution method	Inversion Results	
			Centroids (length,width & time)	Remarks
A	Rupture speed $.7v_S$; grid slips once, M_0 set to known value	SVD	8.7,2.7,13.4	Excellent fit to seismograms; many negative moment rates; final moment poorly reproduced; source time function good, with no negative values
B	Rupture speed $.7v_S$; grid slips once, M_0 set to known value; smoothed 1st der. with weight of 4.	SVD	8.4,2.4,13.0	Excellent fit to data; some negative moment rates final moment well reproduced; source time function good with no negative values, some oscillations around input values
C	Rupture speed $.7v_S$; grid slips more than once, M_0 preset;	"	8.3,2.5,13.0	Excellent fit to data; some negative moment rates final moment & source time ; good with function poorly reproduced
D	Rupture speed $.7v_S$; grid slips once, M_0 preset;	LP	same as input	Excellent fit to data, all aspects of solution exactly reproduced
E	Rupture speed $.7v_S$; grid slips more than once, M_0 preset;	LP	same as input	Excellent fit to data, all aspects of solution exactly reproduced for all practical purposes
F	Rupture speed v_S; grid slips more than once, M_0 preset;	LP	same as input	Excellent fit to data, all aspects of solution exactly reproduced for all practical purposes
G	Rupture speed v_P; grid slips more than once, M_0 preset;	LP	same as input	Excellent fit to data, all aspects of solution exactly reproduced for all practical purposes

Fault strike=0°; dip=30°; rake=90°; Top of fault located at a depth of 5km.

Input parameters:

Number of grids along fault length= 128; number of grids along fault width= 32 ; number of source time steps=26.

Spatial grid size Δx=156.25m; temporal grid size Δt=.1s

Spatial centroid located at center of fault at edge between 8th and 9th grid along length(8.5) and between 2nd and 3rd grid(2.5) along width

Temporal centroid located at $13.2\Delta t$.

Rupture speed =$.7v_S$; each grid slips only for one time step

Inversion parameters:

Number of grids along fault length= 16; number of grids along fault width= 4 ; number of source time steps=26;

Spatial grid size Δx=1.25km; Temporal grid size Δt=.4s

Fault geometry

Thrust fault

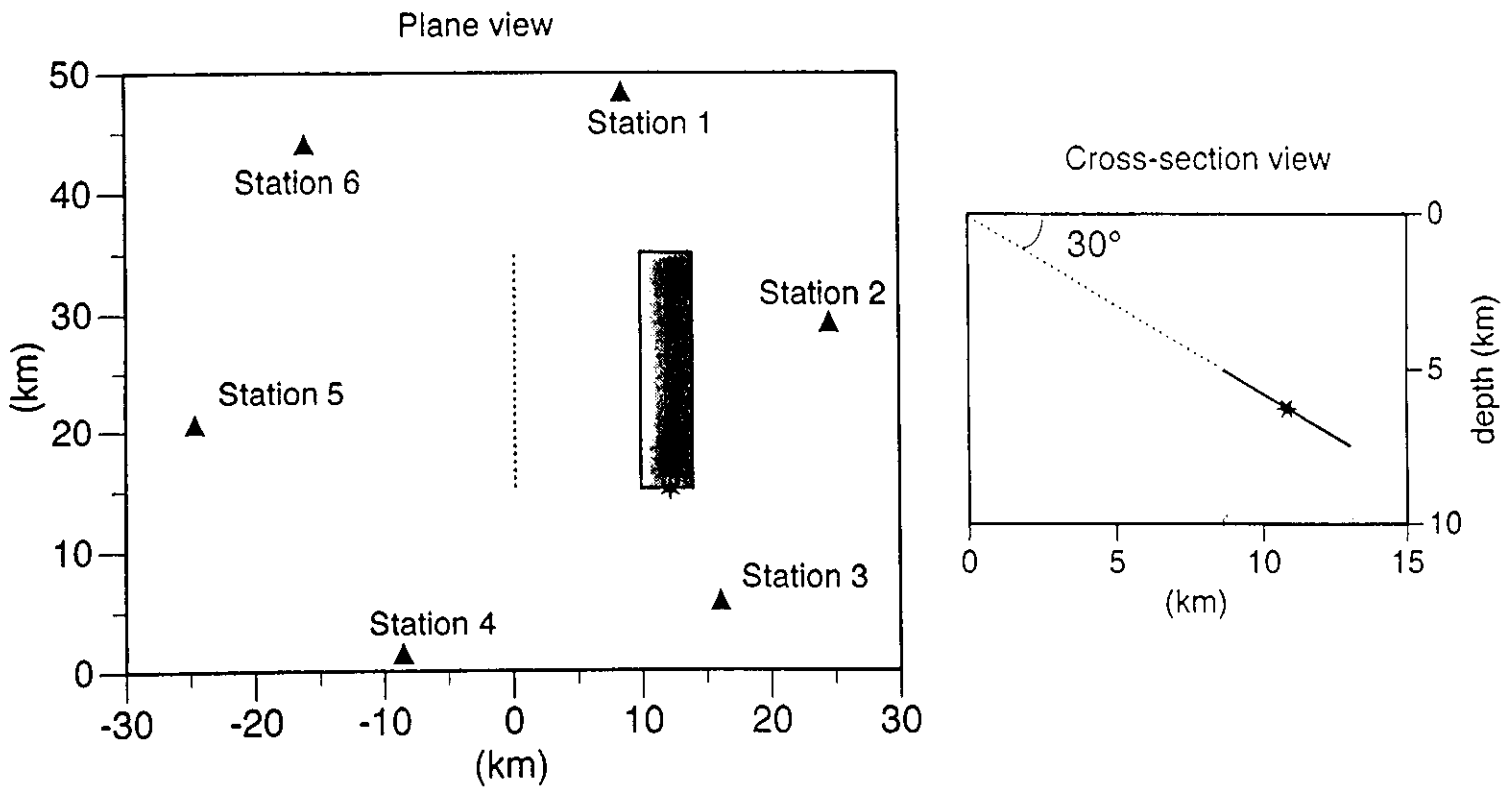

2

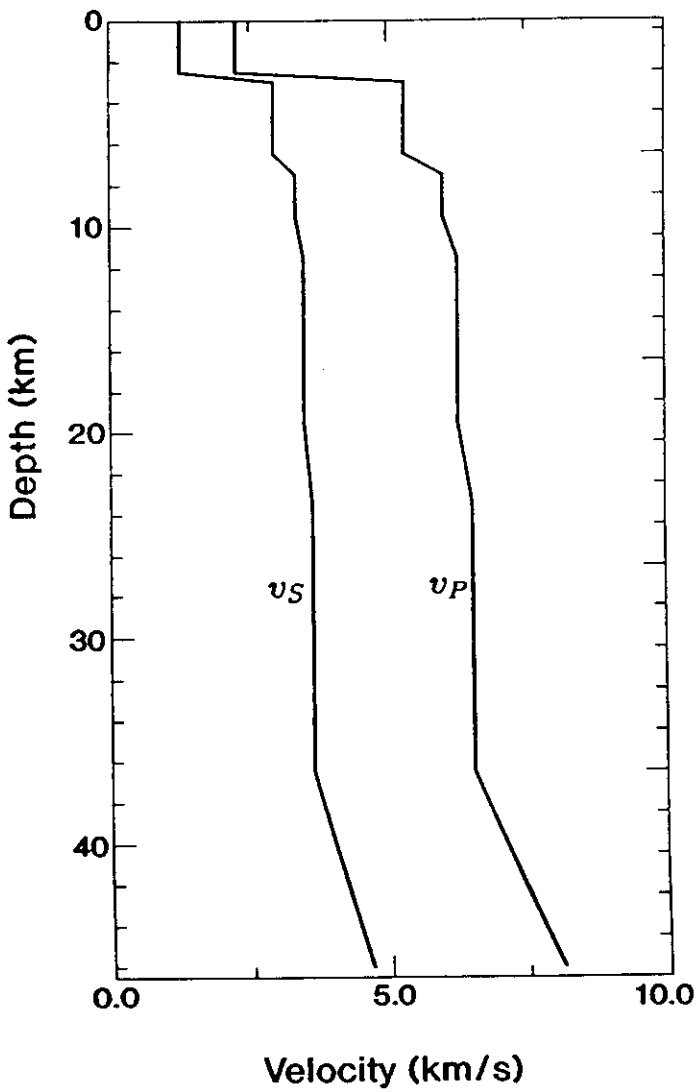

3

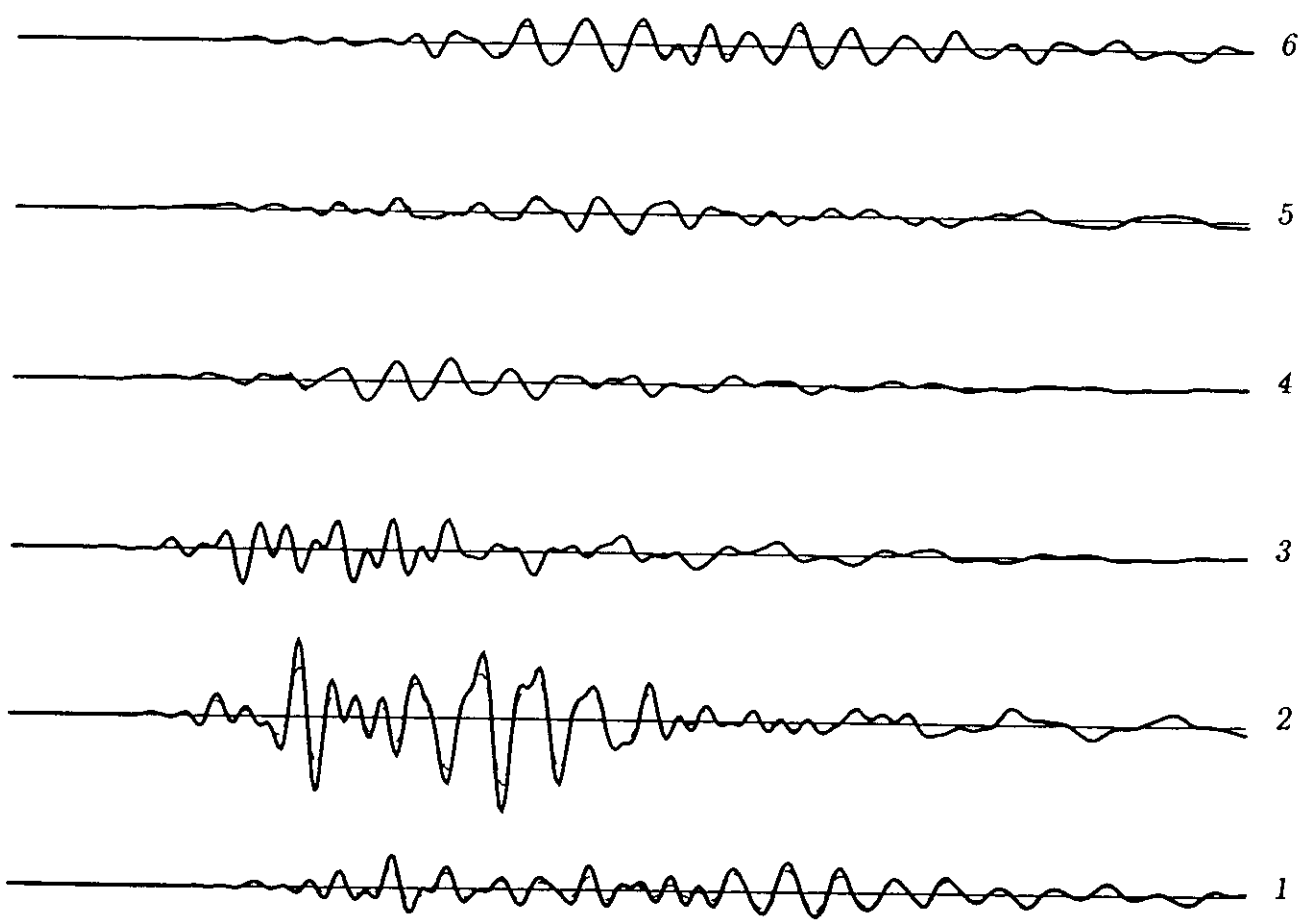

1

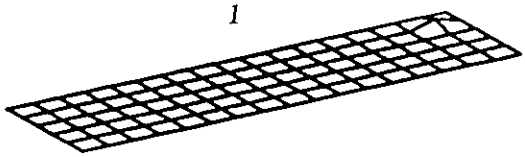

2

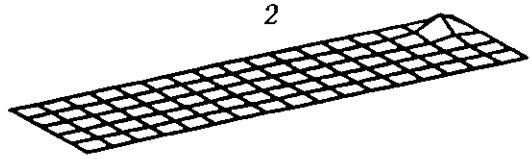

3

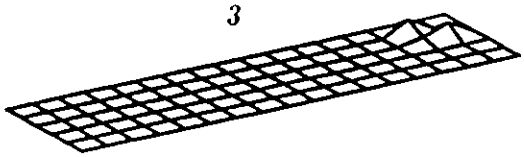

4

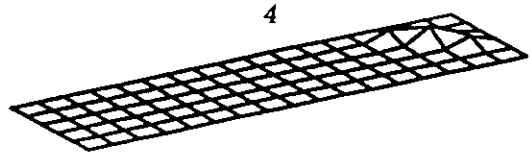

5

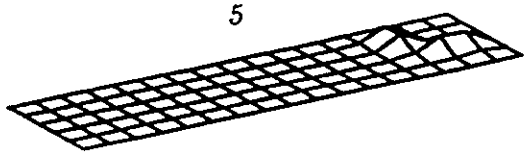

6

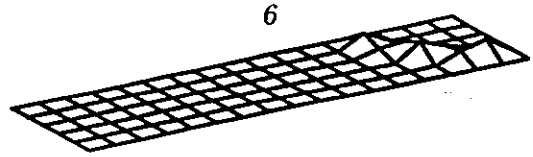

7

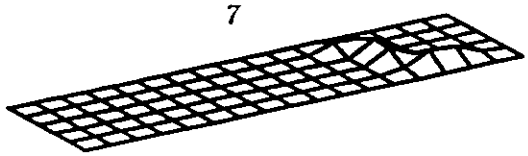

8

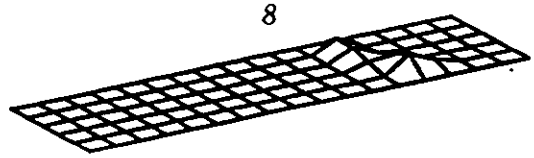

9

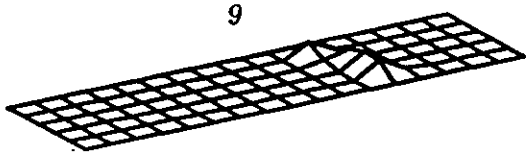

10

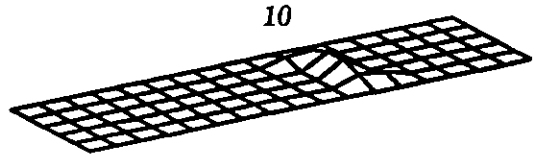

4

cont'd

11

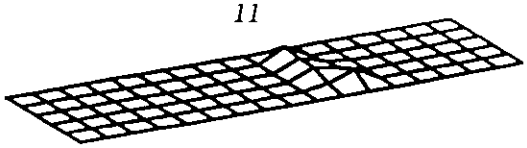

12

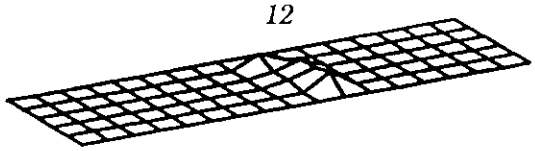

13

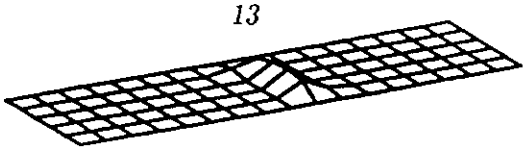

14

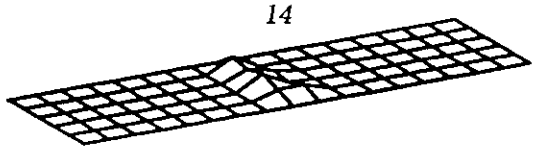

15

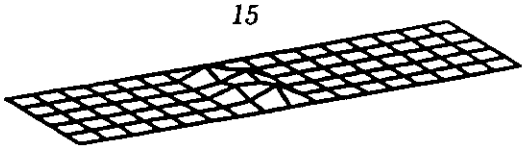

16

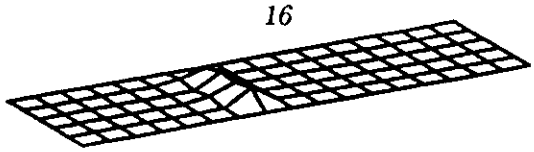

17

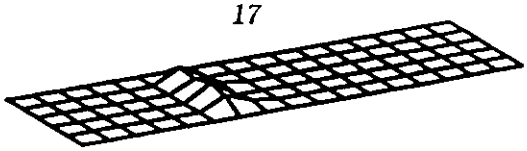

18

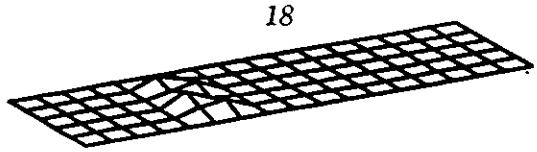

19

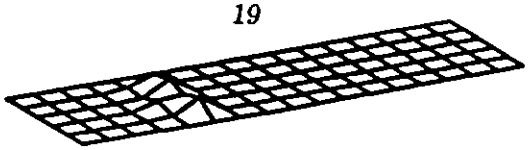

20

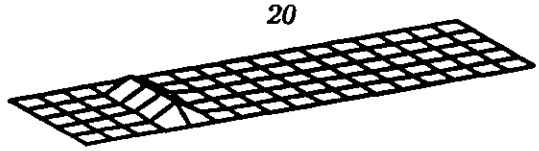

4

cont'd

21

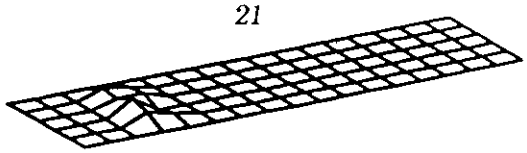

22

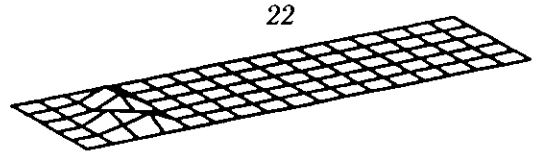

23

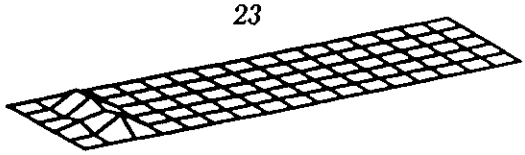

24

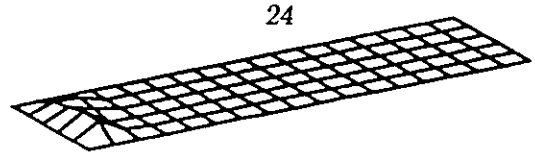

25

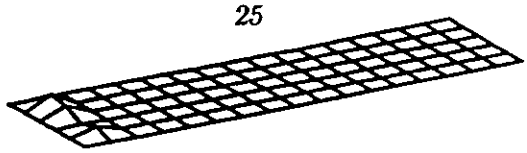

26

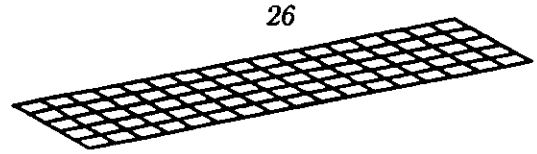

5

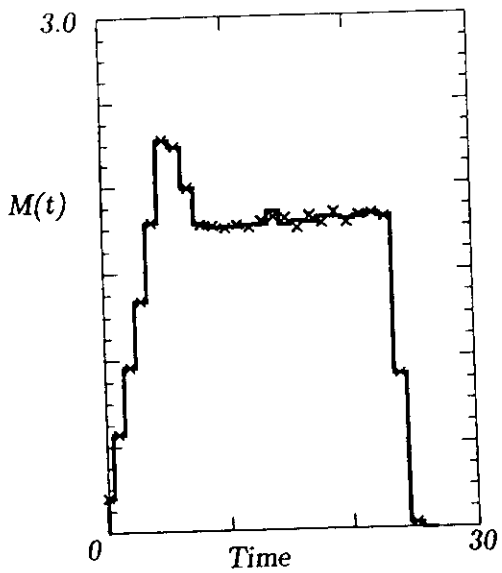

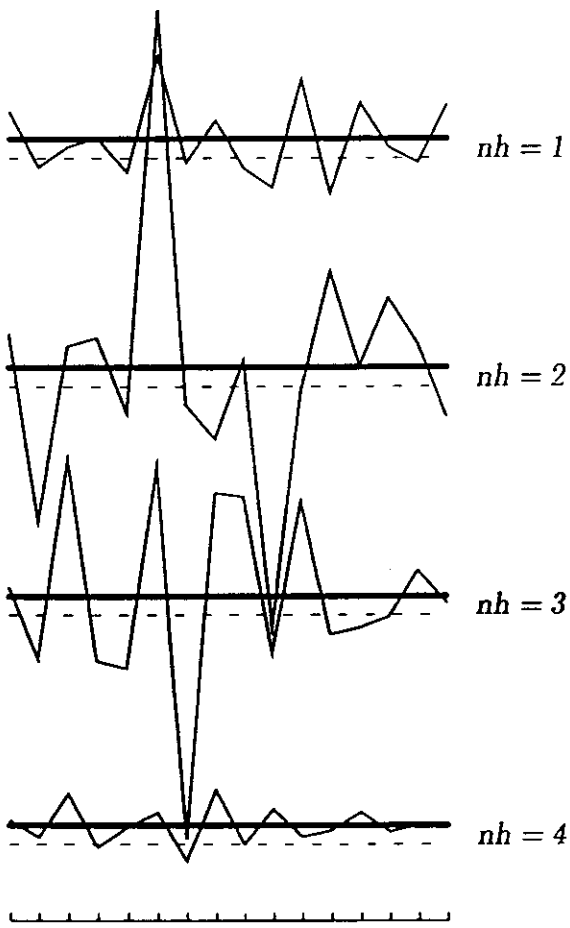
nh = 1
nh = 2
nh = 3
nh = 4


nh = 1


nh = 2

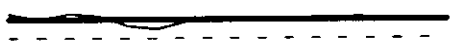
nh = 3


nh = 4

Case A

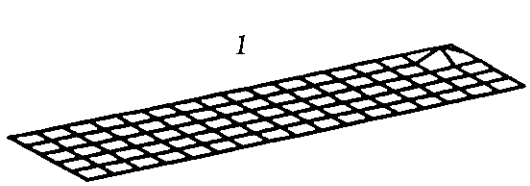

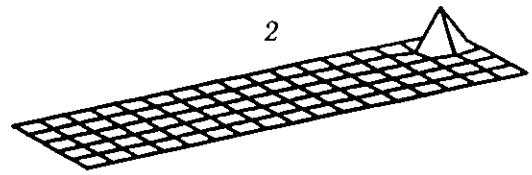

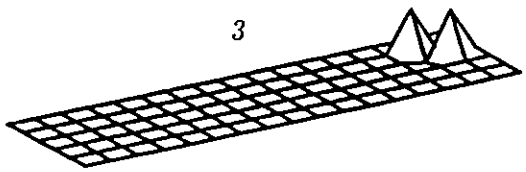

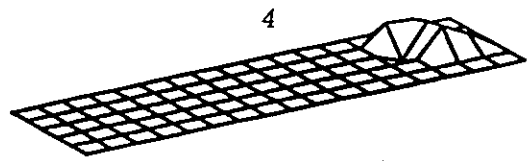

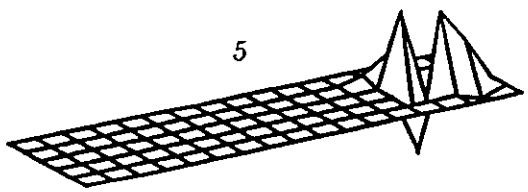

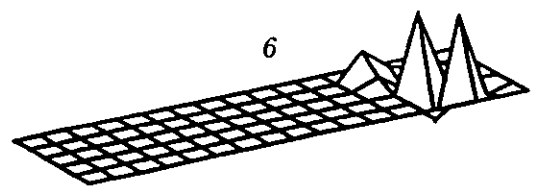

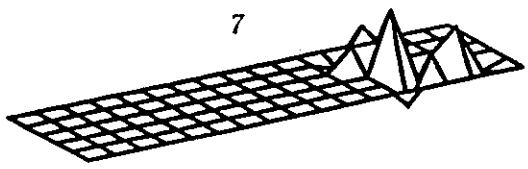

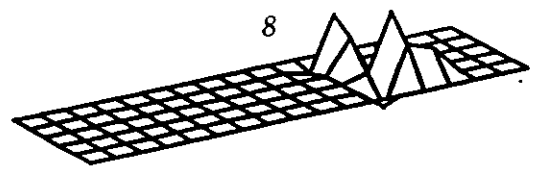

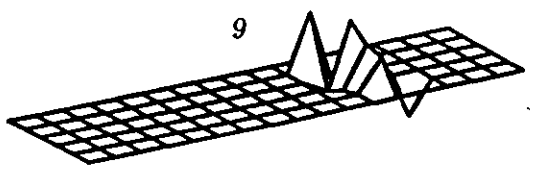

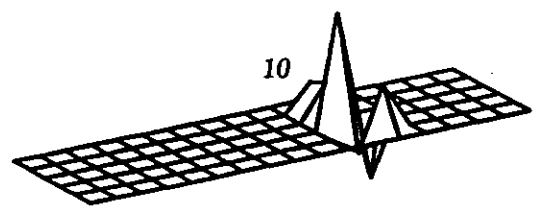

Case A

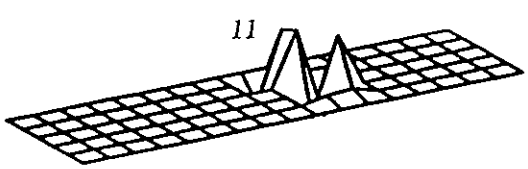

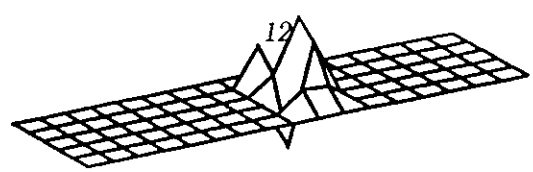

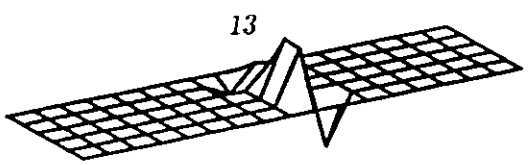

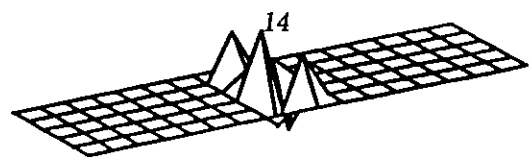

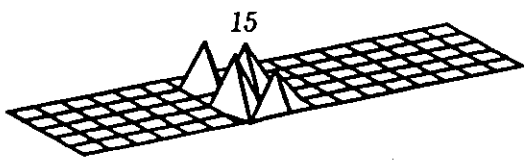

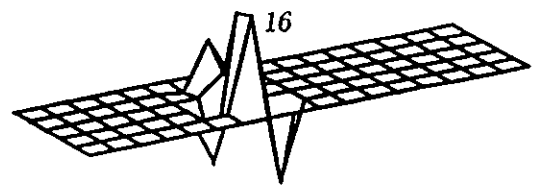

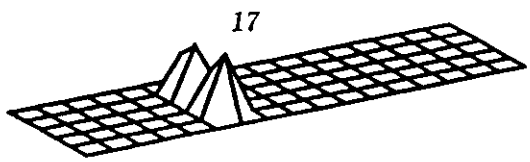

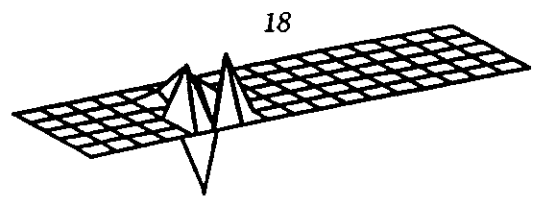

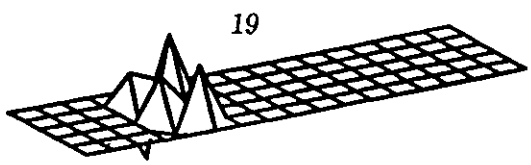

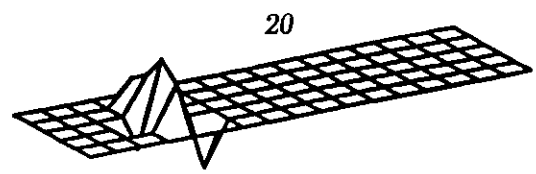

Case A

21

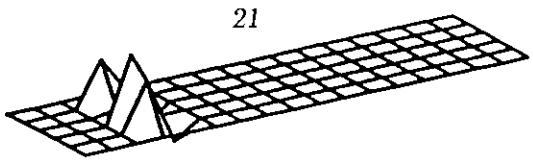

22

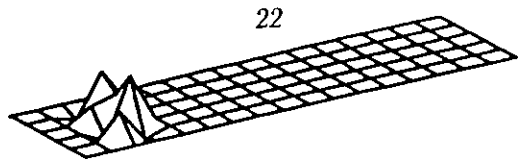

23

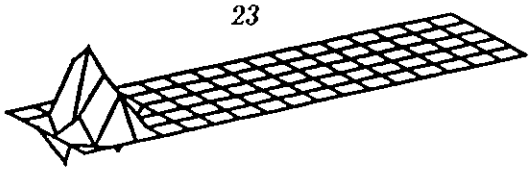

24

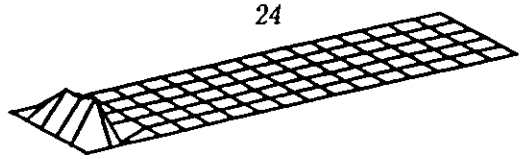

25

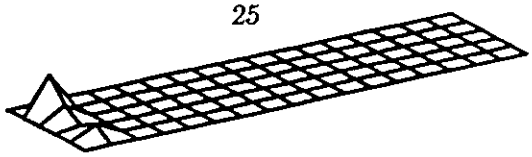

26

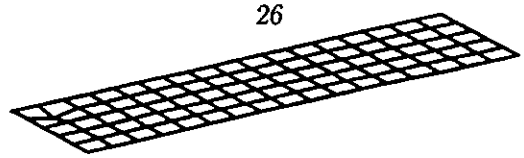

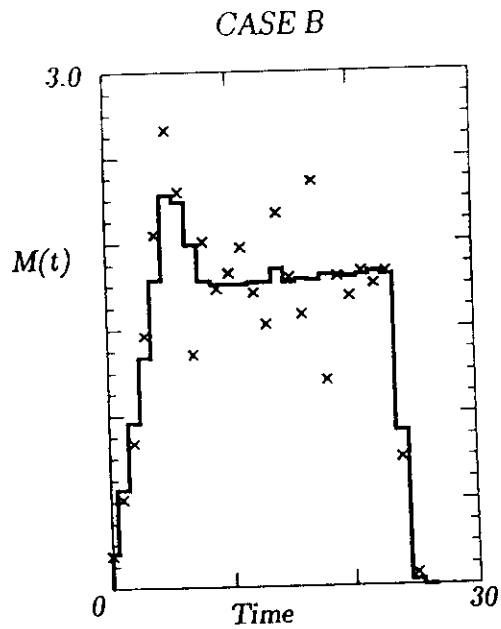
CASE B
3.0
M(t)
0
Time
30

Case C

1

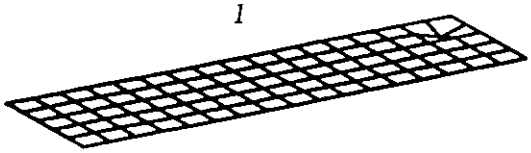

2

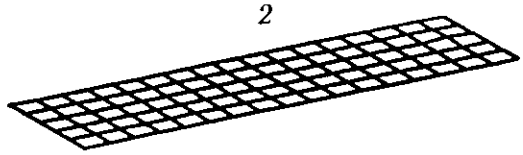

3

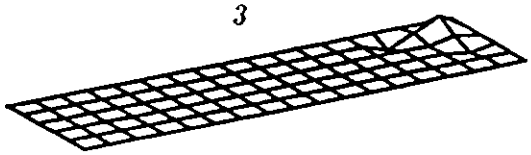

4

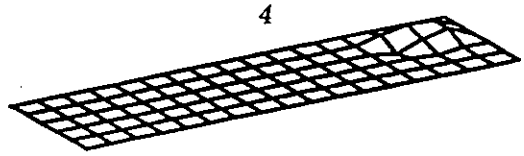

5

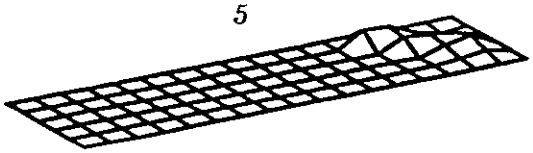

6

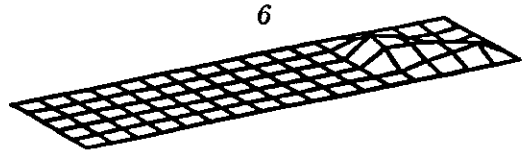

7

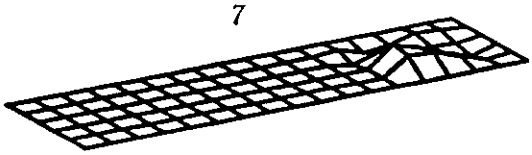

8

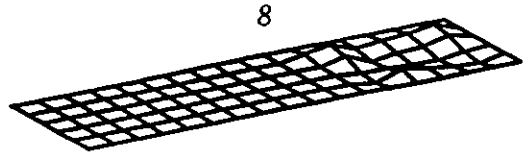

9

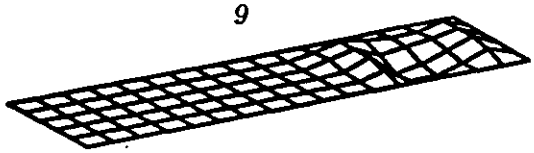

10

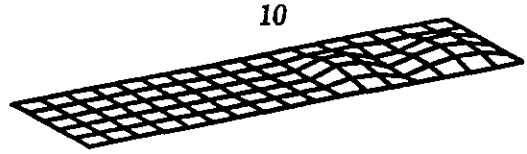

Case C

11

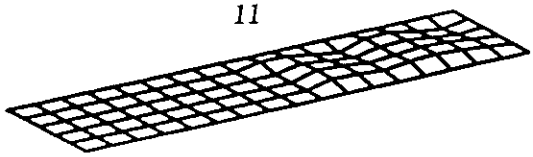

12

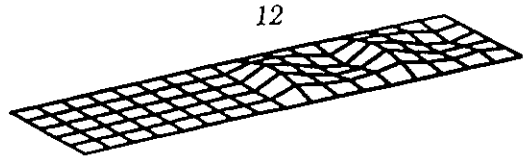

13

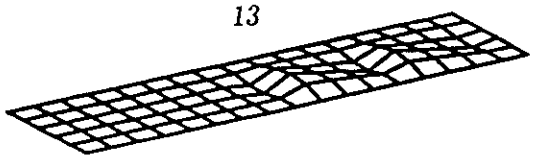

14

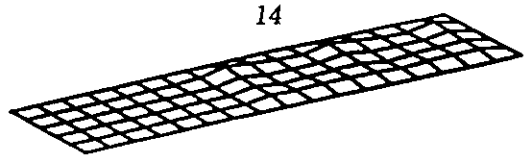

15

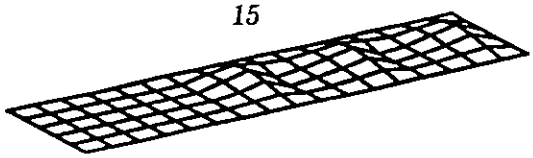

16

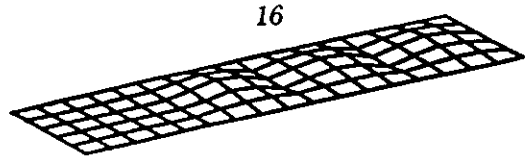

17

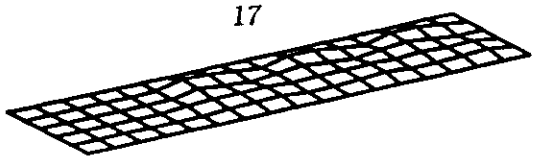

18

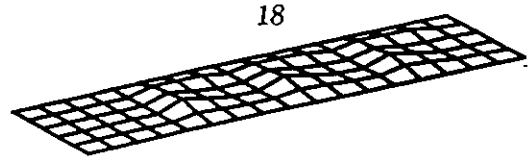

19

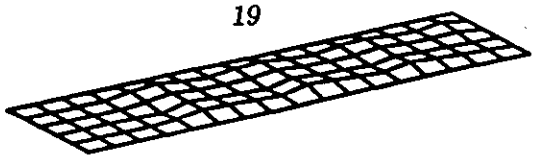

20

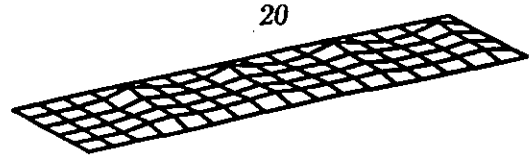

Q10

could

Case C

21

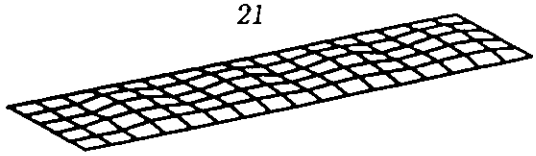

22

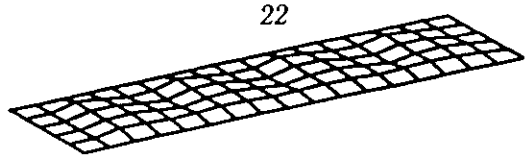

23

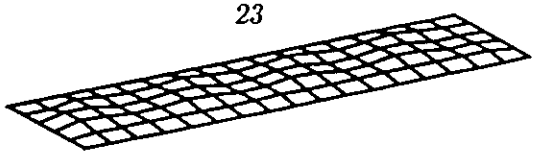

24

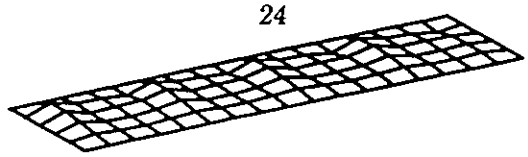

25

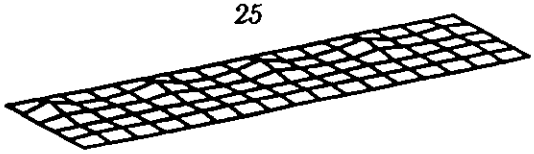

26

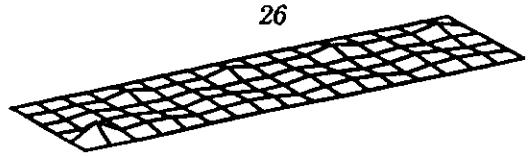

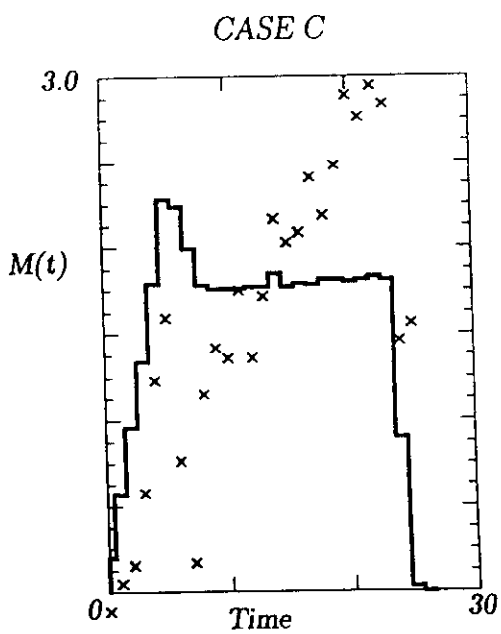
CASE C
3.0
M(t)
0
Time
30

CASE C

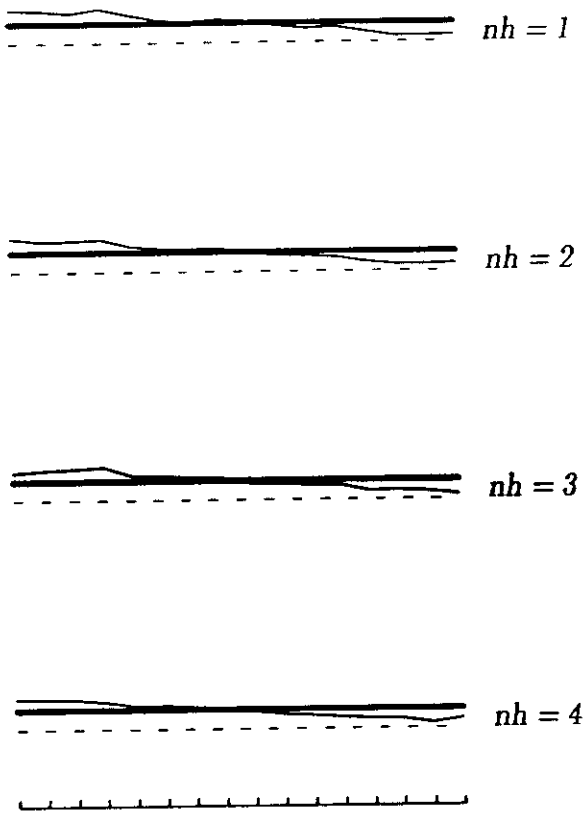

Case E

1

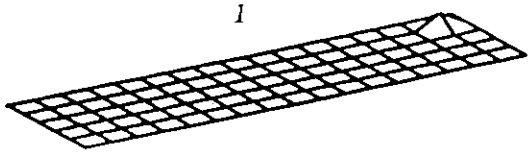

2

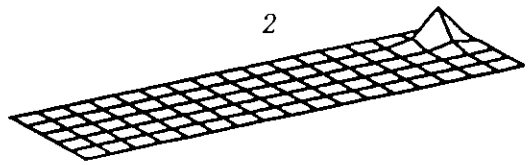

3

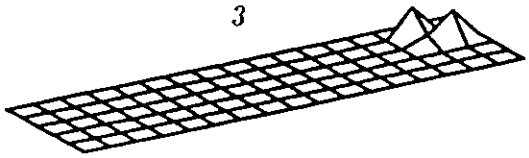

4

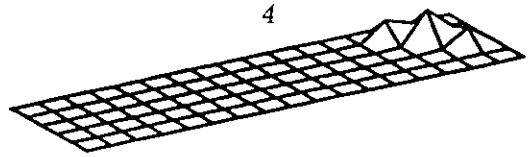

5

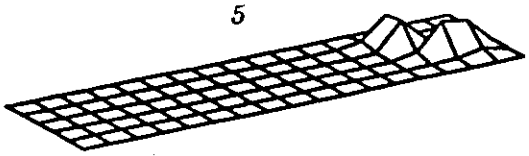

6

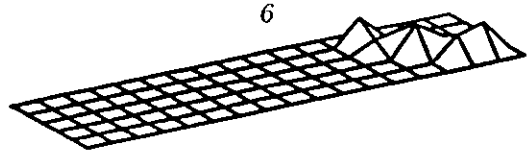

7

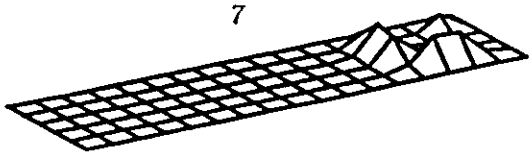

8

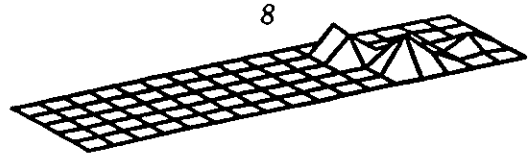

9

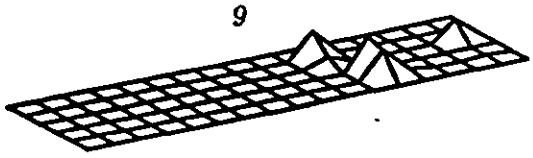

10

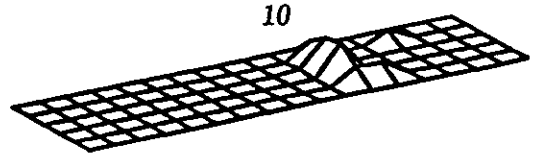

Case E

11

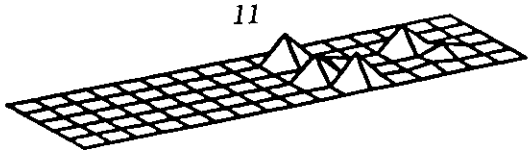

12

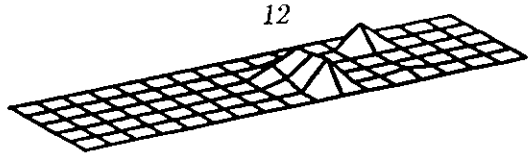

13

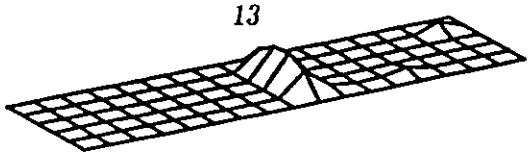

14

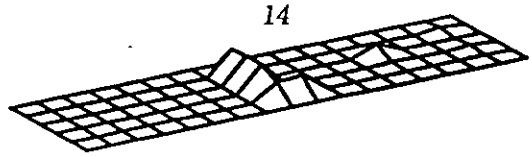

15

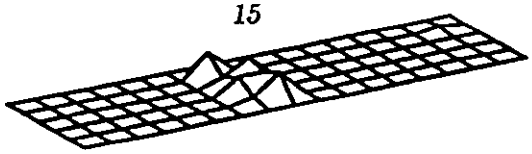

16

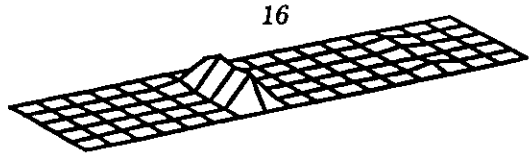

17

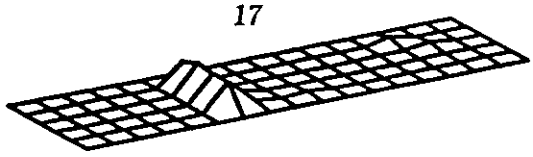

18

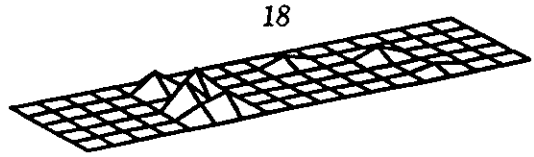

19

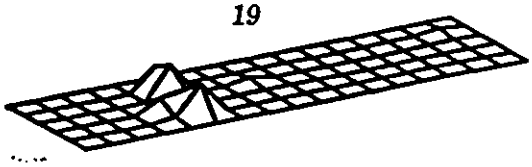

20

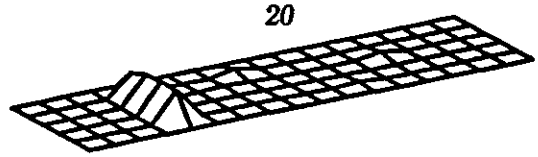

Case E

21

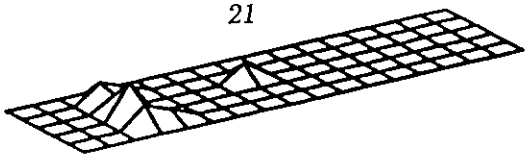

22

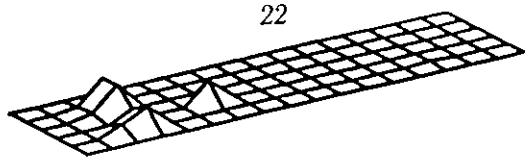

23

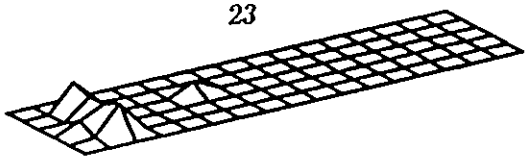

24

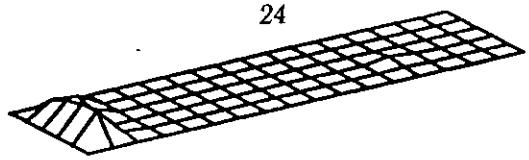

25

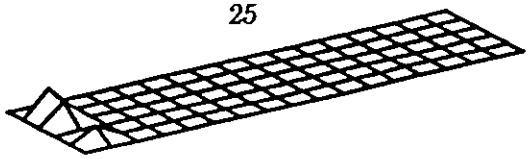

26

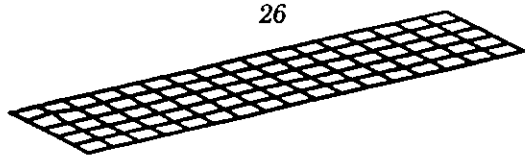

Case F

1

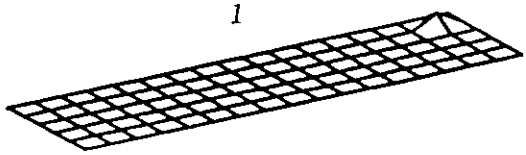

2

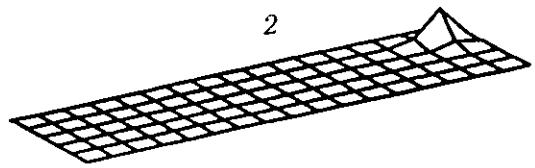

3

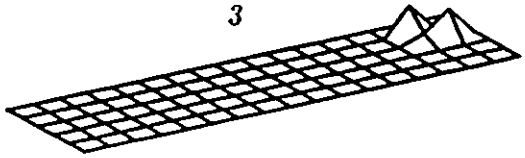

4

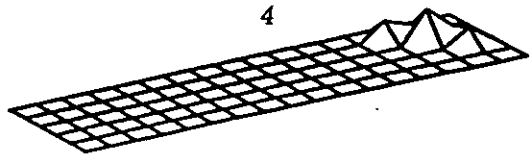

5

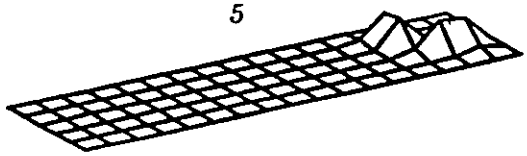

6

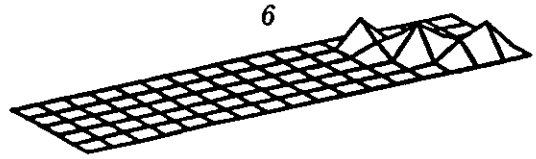

7

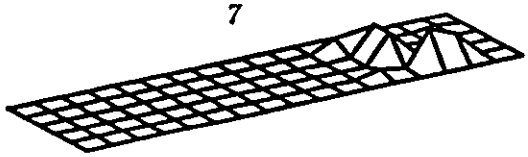

8

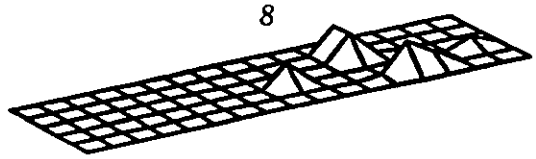

9

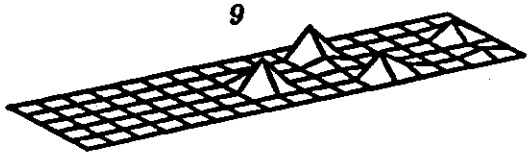

10

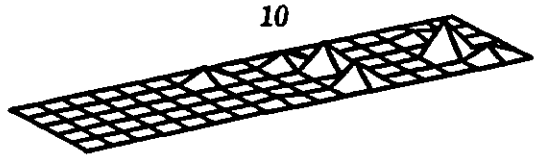

Case F

11

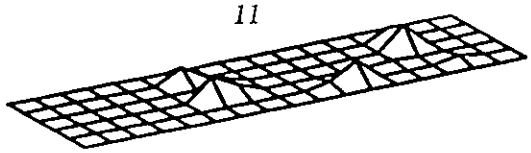

12

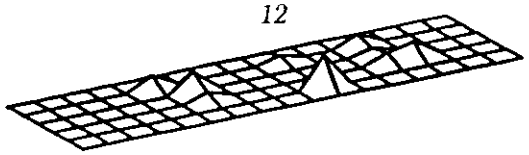

13

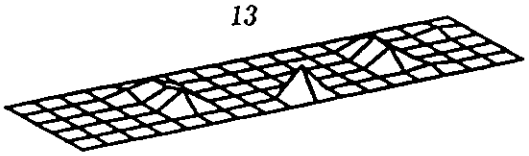

14

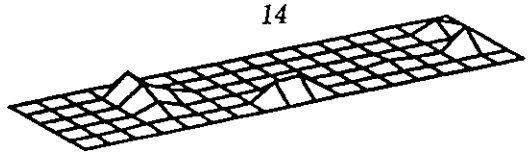

15

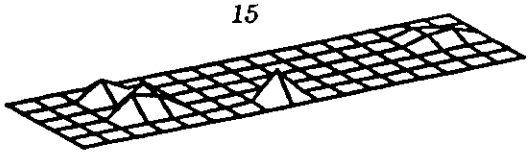

16

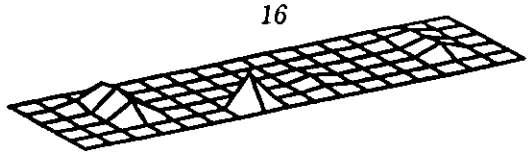

17

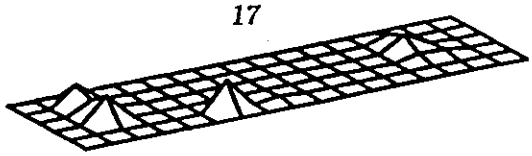

18

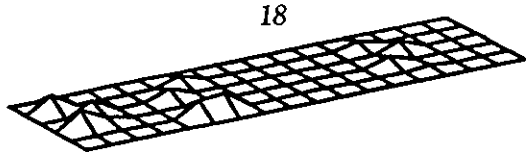

19

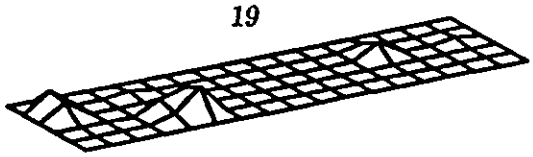

20

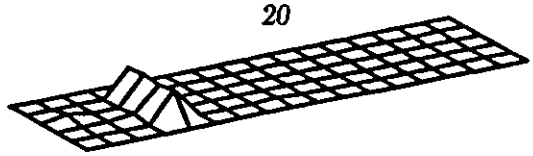

Case F

21

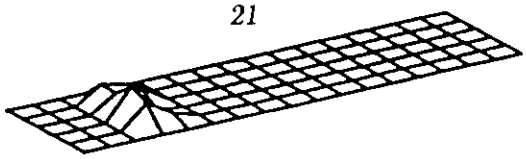

22

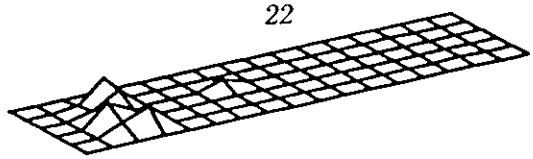

23

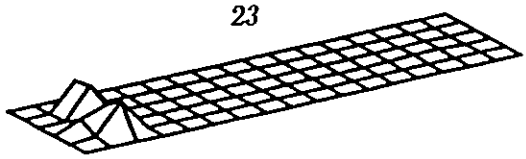

24

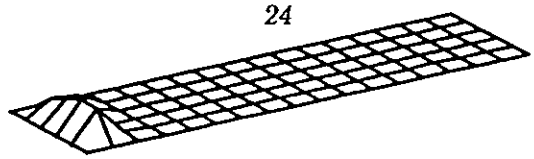

25

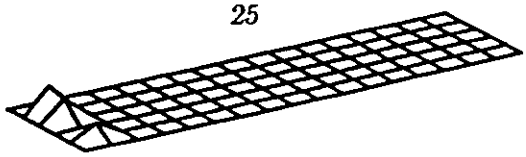

26